角田幸秀

（非会員） 1954年7月6日生。1979年3月岐阜大学工学部電子工学科卒業。工学士。現在，国立循環器病センター研究所，人工臓器部特任研究員，人工臓器，医療計測機器分野の研究に従事。日本人工臓器学会，日本生体医工学会等の会員。

西中知博

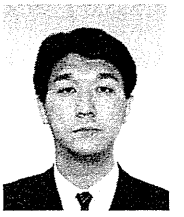

（非会員） 1965年9月3日生。1991年北海道大学医学部医学科卒業。医師。医学博士。現在，東京女子医科大学心臓血管外科，助教授。人工臓器，心臓外科分野の研究に従事。日本人工臓器学会，米国人工臓器学会，日本外科学会，日本胸部外科学会等の会員。

片桐伸将

（非会員）1973年12月2日生。1998年職業能力開発大学校修士課程修了。工学修士。現在，国立循環器病センター研究所，人工臓器部，流動研究員。人工肺の開発，移動現象の数値解析に関する研究に従事。日本人工臓器学会，日本生体医工学会，米国人工臓器学会等の会員。

越地耕二

（正員） 1947年7月5日生。1978年東京理科大学大学院理工学研究科電気工学専攻博士後期課程修了。工学博士。現在，東京理科大学大学院理工学研究科電気工学専攻。教授。電波システム工学，医用電子工学の研究に従事。米国人工臓器学会，日本人工臓器学会等の会員。

人工心臓(基礎)

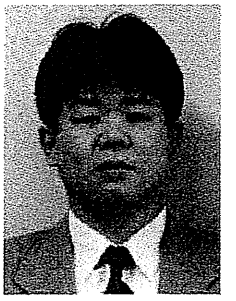

国立循環器病センター研究所先進医工学センター人工臓器部
本間 章彦
Akihiko HOMMA

1. はじめに

医療機器としての人工心臓は，抗血栓性，抗溶血性，解剖学的適合性，制御性，送脱血管，体外装置，価格など，様々な要素を含んだシステム全体としての性能が求められる。高耐久性，抗溶血性，抗血栓性の面から磁気浮上型など，非接触軸受を有する機構が注目されるのは当然であるが，数値流体解析，材料，表面処理技術などを駆使した設計により，各様式における完成度を高めることで優れた性能や臨床成績を実現しているデバイスも存在している。本稿では人工心臓(基礎)として，様々な特色を持つデバイスごとに，最近の報告からその開発動向について述べる。

2. 左心補助人工心臓，補助循環用ポンプの開発動向

HeartAssist 5 (MicroMed Cardiovascular, Inc) はセラミック軸受を有する軸流ポンプであり，重量92 g，大きさ71×30 mm，拍出流量1～10 *l*/minである。対象は小児(18 kg)から成人までで，今まで440人以上の患者に使用されている。電池2個で6～8時間の駆動が可能であり，送血管には流量計を備え，2009年より欧州において遠隔監視システムが使用可能予定となっている。

HeartWare (HeartWare, Inc.) は動圧・磁気ハイブリッド軸受を有する遠心ポンプであり，重量145 g，容積45 ml，拍出流量は上限10 *l*/minとなっている。2008年9月にCEマーク申請。回転数，電流値，血液粘性値を用いた流量推定や吸い付き検出，スラスト軸受部分のCFD，応力解析が行われている。慢性動物実験において，抗凝固療法なしで90日間，耐久性試験では4例で670日以上の駆動を実現している[1]。

Levacor (WorldHeart Corporation) は磁気浮上型遠心ポンプであり，重量440 g，直径75 mm，厚さ35 mmで，電池(400 g)で4時間の駆動が可能である。QOLを考慮した装着様式が検討されている。最終前臨床動物試験において血栓や溶血はみられず，補助流量3～6 *l*/minを維持した[2]。米国での臨床試験は承認を待ち，2008年後半に開始予定。

DuraHeart (Terumo Heart Inc.) は磁気浮上型遠心ポンプであり，重量は540 g，直径72 mm，厚さ54 mmで，拍出流量は10 *l*/minである。慢性動物実験の最長運転期間は864日である。2007年2月にCEマークを取得，米国では2008年7月に最初の埋め込みが実施され，日本では2008年10月より臨床試験を開始した。

VentrAssist (Ventracor Limited) は動圧軸受を有する遠心ポンプで，重量298 g，直径60 mmで，血液接触面にDLCコーティングを施している。2006年11月にCEマークを取得，16歳以下の小児への埋め込みも行われた。現在，米国での臨床試験(BTT，DT)に向けて準備中である。

INCOR (Berlin Heart GmbH) は磁気浮上型軸流ポンプであり，重量200 g，直径30 mm，長さ12 cm，容積82 mlであり，本体に流量推定機能を有している。2003年3月にCEマークを取得し，2006年10月には埋め込み症例数が300例に達し，2008年8月には64歳の男性が埋め込み期間5年目を迎えている。

HeartMate II (Thoratec Corporation) は動圧軸受を有する軸流ポンプで，重量400 g，2005年にCEマークを取得している。ポンプ回転数と消費電力による拍出流量推定が行われている。装着患者が金属製ドアノブへの接触時や電気毛布使用時に皮膚に感じる不快感と対策が報告されている。

■ 著者連絡先
国立循環器病センター研究所先進医工学センター人工臓器部
(〒565-8565　大阪府吹田市藤白台5-7-1)
E-mail. honma@ri.ncvc.go.jp

MiTiHeart (MiTiHeart Corporation) は動圧・磁気ハイブリッド軸受を有する遠心ポンプで，重量640 g，直径50 mm，長さ80 mmで拍出流量は2～10 *l*/minである。DLCコーティングチタン製軸受による耐久性向上や，ヘパリン処理による血液適合性に関する検討が行われている[3]。

Jarvik 2000 (Jarvik Heart, Inc.) はピボット軸受を有する軸流ポンプで，2000年4月より米国と欧州において200人以上の患者に使われている。2005年4月にCEマーク取得(BTT, DT)，FDA承認は現在BTTのみとなっている。最長埋め込み例は7年半(2000年6月～2007年11月)である。日本においても2005年より適用が開始されている。

HeartMate Ⅲ (Thoratec Corporation) は磁気浮上型遠心ポンプであり，重量500 g，直径69 mm，長さ30 mmであり，電池2個で6時間駆動が可能である。HeartMate XVEと同様に焼結チタンを使用し，インペラを除く血液接触面にテクスチャを有する。回転数変化による拍動流発生に関する検討も行われている。慢性動物実験で平均実験期間85日，平均拍出流量6 *l*/minであった[4]。

Baylor Gyro Pump (Baylor College of Medicine) はセラミックと高分子ポリエチレンを使用したダブルピボット型遠心ポンプであり，1995～2004年のNEDOプロジェクトにおいて開発が行われた。凝固系および血小板付着の活性化に対するインペラ表面の粗さの影響について検討している[5]。

The Synergy Pocket Circulatory Assist Device (CircuLite, Inc.) は重量25 g，大きさ14×49 mmの単3乾電池大ポンプで，充填血液量1.7 m*l*，最大拍出流量は3 *l*/minである。鎖骨下埋め込み，左心房脱血，鎖骨下動脈送血であり，長い脱血管は血管内を通じて左心房へ導入される。慢性動物実験で最長埋め込みは300日以上，臨床評価で最長補助期間は213日である[6]。

EVAHEART (サンメディカル技術研究所) は独自のクールシールシステムを有する遠心ポンプで，2008年2月13日までに5施設17症例の治験を実施し，14名が継続中である。そのうち7名が退院・自宅療養で，2名が装置装着状態で就労復帰している。平均補助期間は385日である。耐久試験18台，臨床治験17例において重大な故障は0である。

茨城大学では，永久磁石と電磁石を併用するハイブリッド型軸受を用いた径方向支持型磁気浮上型遠心ポンプの開発を行っている。最大揚程188 mmHg，最大拍出流量14 *l*/minである。また，ラジアル方向支持型磁気浮上遠心ポンプの開発も行っており，直径78.5 mm，長さ41.5 mm，最大揚程250 mmHg，最大拍出流量15 *l*/minである。非定常CFD解析によるポンプ内の流れ，浮上インペラにかかる流体力に関する検討を行っている。さらに小型磁気浮上斜流ポンプの開発も行っている。最大揚程157 mmHg，最大拍出流量4.0 *l*/minである。3次元磁場解析による発生吸引力の推定，磁気飽和回避等の検討を行っている。

東京電機大学と杏林大学では，円錐型スパイラル溝付動圧軸受を用いたエンクローズド型軸流血液ポンプの開発を行っている。軸受の基礎特性測定，エンクローズドインペラのCFD解析，磁場解析によるポンプモータ形状の検討も行っている。

東京大学，東北大学らのグループは円板の揺動運動により血液を拍出する波動ポンプを用いたUPVADの開発を行っている。直径72 mm，厚さ32.5 mm，重量33 gである。慢性動物実験での最長生存期間は276日である。脱血管部の圧力センサーによる吸い付き防止制御法が検討されている。

動圧軸受けを有する軸流型補助人工心臓ポンプ(三菱重工業株式会社)は直径29 mm，長さ70 mmであり，揚程100 mmHg，回転数9,000 rpmにて拍出流量5 *l*/minの性能を有している。慢性動物実験で90日間の生存記録を得ている。

東京医科歯科大学，東京工業大学，芝浦工業大学らのグループによって，Bio-Pump (Medrtonics, INC.) の機械軸受を磁気軸受に置き換えた磁気浮上遠心血液ポンプ(Mag-Lev Bio-Pump)の試作検討が行われている。

東京工業大学，東京医科歯科大学らのグループによって，径方向の能動的制御を行う磁気浮上遠心血液ポンプ(MedTech Heart)の開発が行われている。直径64 mm，厚さ32 mmであり，磁気軸受とモータ構造が別で高剛性という特徴を持っている。

産業技術総合研究所では，動圧軸受によりインペラの非接触回転浮上を実現するセミオープンタイプ型遠心ポンプ(AIST hydrodynamically-levitated centrifugal pump)の開発が行われている。軸方向隙間，磁力，ステップ動圧軸受を変えた比較検討や24時間の慢性動物実験評価を行っている。

杏林大学，東京電機大学，国立循環器病センターらのグループによって，リニアアクチュエータを用いた拍動流ポンプlinear LVASの開発が行われている。linear LVASは重量740 g，直径100 mm，厚さ50 mmである。慢性動物実験で装置故障は一切確認されず，42日間の生存を記録している。

国立循環器病センターでは，次世代体内埋め込み型空気駆動式補助人工心臓システムの開発が行われている。弁の

取付方向が血液ポンプ内の流れに与える影響や，弁の種類や動作によるキャビテーション発生について検討を行っている。

産業技術総合研究所，泉工医科工業らのグループによって，インペラを1点のピボット軸受けとラジアル型磁気カップリングで支持し，2週間程度の使用を目指した補助循環用モノピボット遠心ポンプ(MERA)の開発と製品化が行われている。

3. 右心補助人工心臓の開発動向

DexAide (Cleveland Clinic) は，CorAideをもとに設計された動圧軸受を有する遠心ポンプである。チタン製とジルコニア製のステータの比較検討を行っている[7]。動物実験による脱血管の検討，LVADにHeartMate XVEおよびCorAideを用いた場合の送脱血管の最適なデザインや埋め込み位置の検討が死体を用いて行われている。

4. 両心補助人工心臓の開発動向

Korea Artificial Organ Center, Korea Universityでは，プッシャープレートで左右ベローズを駆動し，左右血液ポンプを駆動するウェアラブル空気駆動型両心補助人工心臓HVAD (Electrical-pneumatic hybrid VAD) の開発が行われている。特性試験では血液ポンプ容積55 m*l*，拍動数60 bpm時に平均拍出流量3.25 *l*/minを得ている[8]。

The Prince Charles Hospital，茨城大学，都城工業高等専門学校らのグループにより，磁気支持型両心補助用人工心臓BIVACORの開発が行われている。上下に左心・右心補助用の羽根を持つインペラが磁気軸受により軸方向に変位し，ケーシング間との距離が変化することで左右拍出性能を制御する仕組みになっている。

5. 全人工心臓の開発動向

プランジャーの往復運動によりプッシャープレート型左右血液ポンプを交互に駆動するMagScrew TAH (Cleveland Clinic) は，弁に牛心嚢膜弁を使用し[9]，各血液ポンプ容積は45 m*l*で，拍動数220 bpm時に最大拍出流量11 *l*/minである。22ヶ月におよぶ外部電池の充放電耐久試験が行われている。

ボイスコイルタイプのリニアアクチュエータにより血液ポンプ駆動するACcor (RWTH Aachen University) は，重量800 g以下で，直径84 mm，長さ94 mm，後負荷100 mmHgに対して6 *l*/min以上の拍出流量を実現している。電磁界解析によるリニアドライブの発生力や効率などの最適化を行っている[10]。また重量470 gで拍出流量4.5～7 *l*/minであるMiniACcor (RWTH Aachen University) の開発も行われている。

東京大学，東北大学らは2つの波動ポンプから成るUPTAH (直径77 mm，長さ78.5 mm) の開発を行っている。慢性動物実験において，生存期間72日間のうち術後14～36日目まで1/R制御により非拍動流による維持が可能であった。

6. 小児用人工心臓，補助循環用ポンプの開発動向

Pediatric Jarvik 2000 (Jarvik Heart, Inc.) はJarvik Heartを小児，新生児用に小型化したピボット軸受を有する軸流ポンプである。5段階の回転数による拍出流量変化幅は小児用で1.57～4.0 *l*/mim，新生児用で0.5～1.2 *l*/minとなっている。慢性動物実験におけるポンプ停止の主要な原因はベアリング部分の血栓形成であり，この部分の改良が今後の課題となっている[11]。

PediaFlow (WorldHeart Inc.) は体重3～15 kgの新生児から小児を対象とした磁気浮上型斜流ポンプである。外径30.5 mm，長さ46 mm，拍出流量0.3～1.5 *l*/minである。Levacor用コントローラーを転用し，システム全体で6ヶ月以上の安定した動作と循環補助を実現している[12]。溶血実験や急性・慢性動物実験評価，CFDやPIVによる流れの解析，ポンプ温度分布に関する有限要素解析が行われている。

Pedipump (Cleveland Clinic) は受動的磁気軸受を有する斜流ポンプで，ローター前後にルビージルコニアを用いた接触点を持つ。血管内用 (4.5×55 mm) と血管外用 (11×70 mm) がある[13]。耐久試験では積算で160，181時間の駆動を実現し，急性・慢性動物実験評価，被験者 (13人，生後2日～13歳11ヶ月) のCT画像を用いた解剖学的適合性に関する検討も行っている。

PediVAS (Levitronix LLC) はCentriMagをベースに開発され，ポンプは一回使用で充填血液量は14 m*l*である。最大回転数5,500 rpm時に拍出流量0.3～3.0 *l*/minになるようポンプ効率を最適化し，慢性動物実験において30日間，循環動態を良好に維持した[14]。

The Penn State Pediatric VAD (PVAD) (The Pennsylvania State University) は，0～9ヶ月の新生児を対象とした空気駆動型拍動式VADで，一回拍出流量は12～16 m*l*/min，Bjork-Shiley弁 (17 mm) を使用している。弁に関する検討 (取り付け角度，種類，キャビテーション発生)，離脱時の低拍動，低流量時の血液の流れ，完全充満・完全駆出に必要な圧力値や時間などについて検討している[15]。

Ultramag (Levitronix LLC) は磁気浮上型遠心ポンプであ

り，小児から成人までを対象としている。直径46 mm以下，高さ7～9 mm，最大回転数9,000 rpm，拍出流量0.5～3.0 *l*/minである。慢性動物実験（子羊，重量15～24 kg）において平均拍出流量は約1 *l*/minで維持され，装置故障はなく29～90日で予定を終了している[16]。

EXCOR Pediatric VAD（Berlin Heart GmbH）は空気駆動型拍動式VADであり，血液ポンプ容積は5種類，カニューレは2サイズ，3種類のバリエーションがある。2007年5月，EXCOR Pediatric VADのIDE study（10施設10例）が開始，同年11月に最初の患者登録（8歳，男子）が行われた。

経皮的補助循環システムであるTandemHeart（動圧軸受を有するパージ方式遠心ポンプ）をもとに，体重2～40 kgの小児を対象に，最長14日間の使用を目的とした小児用ポンプThe pediatric TandemHeart pump（CardiacAssist, Inc.）の開発が行われている。インペラの直径は40 mm，充填血液量は4 m*l*である。揚程250 mmHgに対し5,500 rpmで2.0 *l*/minの性能を示している[17]。

東京医科歯科大学，芝浦工業大学らのグループは，磁気カップリング駆動の小型遠心ポンプTinyPumpの開発を行っている。充填血液量は5 m*l*，拍出流量は0.1～1.5 *l*/min，体重3.5～10 kgの新生児や小児への適用を目指している。また体外循環やECMO用としてディスポーザブル式"TinyPump" Dispoの開発も行っている。

以上，速報性を重視し学会大会の演題を中心にまとめた。発表時のデータを採用している部分は，論文集などのデータと若干異なっていることをご容赦願いたい。

文　献

1) Reyes C, Bleyer P, Benitez M, et al: Life-Cycle Testing of the HeartWare Left Ventricular Assist Device. ASAIO J 54: 57A, 2008
2) Bearnson G, Miller P, Jacobs G, et al: WorldHeart Levacor VAD: Clinical Readiness for US Trial. ASAIO J 54: 38A, 2008
3) Jahanmir S, Ren Z, Hunsberger AZ, et al: Status of the Magnetically Levitated MiTiHeart LVAD. ASAIO J 54: 22A, 2008
4) Farrar DJ, Bourque K, Dague CP, et al: Design features, developmental status, and experimental results with the Heartmate III centrifugal left ventricular assist system with a magnetically levitated rotor. ASAIO J 53: 310-5, 2007
5) Linneweber J, Dohmen PM, Kertzscher U, et al: The effect of surface roughness on activation of the coagulation system and platelet adhesion in rotary blood pumps. Artif Organs 31: 345-51, 2007
6) Marseille O, Kerkhoffs W, Meyns B, et al: Cannula development of the circulite synergy micro-pump system for partial circulatory support. ASAIO J 54: 44A, 2008
7) Saeed D, Horvath DJ, Massiello AL, et al: In vitro evaluation of zirconia ceramic in the Dexaide right ventricular assist device journal bearing. ASAIO J 54: 23A, 2008
8) Jeong GS, Hwang CM, Nam KW, et al: Hydrodynamics characteristics of wearable pneumatic bi-ventricular assist device. 第45回日本人工臓器学会大会予稿集 36: S-88, 2007
9) Flick CR, Weber S, Luangphakdy V, et al: Pressures generated within the chambers of the MagScrew TAH: an in vitro study. ASAIO J 54: 58-63, 2008
10) Finocchiaro T, Lessmann M, Körfer R, et al: New drive concept for the Aachen total artificial heart "ACcor". ASAIO J 54: 43A, 2008
11) Wu ZJ, Cheng G, Burgreen GW, et al: Progress and In-vitro experience of the pediatric Jarvik 2000 Hearts. 第45回日本人工臓器学会大会予稿集 36: S-3, 2007
12) Verkaik J, Snyder S, Paden D, et al: Towards the development of the 2nd generation (GEN2) PediaFlow Pediatric VAD. ASAIO J 54: 33A, 2008
13) Weber S, Saeed D, Dudzinski D, et al: The PediPump: a versatile, implantable pediatric ventricular assist device-update IV. ASAIO J 54: 46A, 2008
14) Dasse KA, Gempp T, Wearden P, et al: Development and evaluation of magnetically levitated systems for pediatric cardiac & cardiopulmonary support. 第45回日本人工臓器学会大会予稿集 36: S-4, 2007
15) Lukir B, Mnning K, Deutsch S, et al: In vitro testing of the Penn State Pediatric VAD (PVAD). 第45回日本人工臓器学会大会予稿集 36: S-4, 2007
16) Taskin ME, Zhang T, Gellman B, et al: Computational flow and blood damage modeling of the ultramag blood pump. ASAIO J 54: 6A, 2008
17) Svitek RG, Smith DE, Magovern JA: In vitro evaluation of the TandemHeart pediatric centrifugal pump. ASAIO J 53: 747-53, 2007

3 B 2-5

完全体内埋込型人工心臓駆動用体外結合型経皮エネルギー伝送システム小型化の検討

Investigation of miniaturizing an Externally-Coupled Transcutaneous Energy Transmission System for a Totally-Implantable Artificial Heart

○本郷孝規[1]，山本隆彦[1]，青木広宙[1]，越地耕二[1]，本間章彦[2]，巽英介[2]，妙中義之[2]

[1]東京理科大学，[2]国立循環器病センター

Takanori HONGO[1], Takahiko YAMAMOTO[1], Hirooki AOKI[1], Kohji KOSHIJI[1],

A. HONMA[2], E. TATSUMI[2], Y. TAENAKA[2]

[1]Tokyo University of Science, Chiba, [2]National Cardiovascular Center, Osaka, Japan

1. はじめに

現在我々は体外結合型経皮エネルギー伝送システム(ECTETS[1])の研究・開発を行っている．患者の精神的・身体的負担を少しでも軽減するため，ECTETSも可能な限り小型、軽量であることが望ましい．現在、スイッチング周波数 300kHz でエネルギー伝送を行っているが、スイッチング周波数の高周波化によって ECTETS の小型化が図れる。本報告では従来より高い周波数でエネルギー伝送が行えるよう回路に改善を加え，伝送周波数高周波化による効用について検討したので報告する．

2. 実験方法

経皮トランスの 1 次(体外)コイルは、トロイダル型の Mn-Zn フェライト(7H20,FDK 社製：外径 38mm、内径 22mm、断面積約 112mm、重量 50g)を磁心とし、1 次コイルの巻き線には、直径 0.05mm のポリウレタン被膜銅線を 120 本一束にしたリッツ線を使用した。また、2 次(体内)コイルは 1 次コイルと同様のリッツ線を直径 42mm の円環状に数回巻いたものを使用した。また測定条件は、出力電力＝20W、巻き数比1：1とした．

現在我々は巻き数 9 回、伝送周波数 300kHz、DC 入力電圧 37V という値を用いてエネルギー伝送を行っている。本報告では ECTETS 体外回路に改善を施し、DC-to-DC エネルギー伝送を測定した。また本測定ではエネルギー伝送周波数を 200kHz 高い 500kHz とし、コイル巻き数の変化に対する DC-to-DC エネルギー伝送効率を測定した。一方、各巻き数毎の、システム終端に 20W の DC 電力を伝送することのできる最低電圧 Vo についても調査した。

3. 結果

巻き数対 DC-to-DC エネルギー伝送効率の特性を Fig.1 に、巻き数対 Vo の特性を Fig.2 に示す。最も効率が高い点は 6 回巻きのときで、効率は85.3%であった。37Vより 3.5V低い約33.5Vの場合でも，システム終端に 20W の DC 電力を供給することができた。この結果，第一にコイル厚みが従来の 9 回巻きから 6 回巻きへと薄型化されること，第二に，現在 DC 電力供給に必要な体外電池のセル数は 10 本であるが，これを 1 本減少させること，等の効果があると考えられる．

4. まとめ・今後の計画

以上より，従来使用していたコアに比べて[1]，遜色のない効率でエネルギー伝送が行えることを確認した．また，小型化の面においては，トランスコイル巻き数を従来の 9 回から6回に薄型化(二次コイル厚み 19.0%減少)，DC 電力供給用の体外二次電池(Fig.3)のセル数を、10 本から 9 本に減少できることを確認した。

今後は，1 次コイル磁心の断面積減少の検討，および本報告で使用したECTETSに対する，エネルギー伝送時の発熱評価を行っていきたいと考えている．

[参考文献]

1)第 19 回「電磁力関連のダイナミクス」講演論文集，p.147

体内埋込型人工心臓駆動用体外結合型経皮エネルギー伝送システム-小型化のためのスイッチング周波数高周波化の検討-

○本郷孝規，山本隆彦，青木広宙，越地耕二

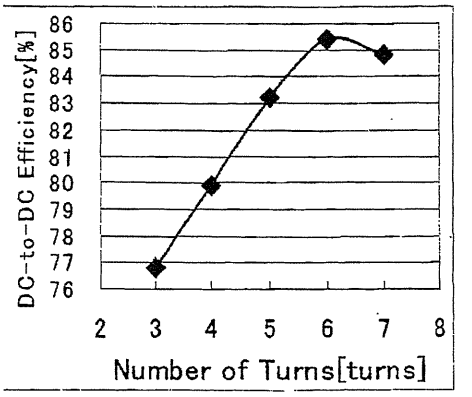

Fig.1 AC-to-AC energy transmission efficiency as a function of number of turns

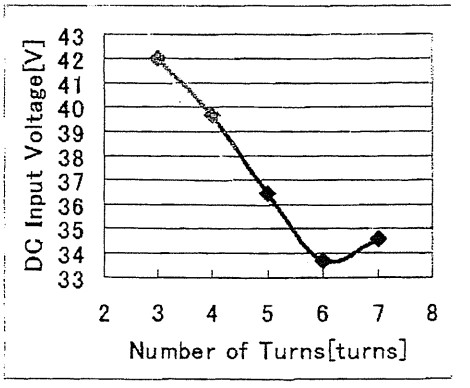

Fig.2 Characteristics of DC input voltage as a function of number of turns

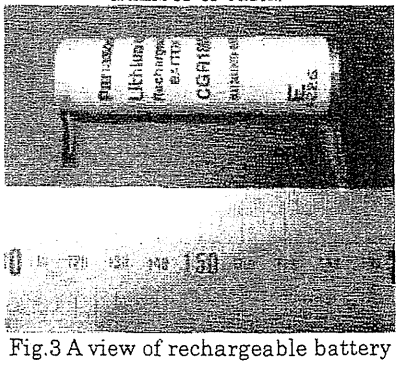

Fig.3 A view of rechargeable battery

Am J Physiol Heart Circ Physiol 296: H1117–H1124, 2009.
First published February 6, 2009; doi:10.1152/ajpheart.01120.2008.

Mechanical work and energetic analysis of eccentric cardiac remodeling in a volume overload heart failure in rats

Yoshiaki Takewa,[1,2,3,4] Elie R. Chemaly,[1,4] Miyako Takaki,[2] Li Fan Liang,[1,4] Hongwei Jin,[1,4] Ioannis Karakikes,[1] Charlotte Morel,[1] Yoshiyuki Taenaka,[3] Eisuke Tatsumi,[3] and Roger J. Hajjar[1,4]

[1]Cardiovascular Research Center, Mount Sinai School of Medicine, New York, New York; [2]Department of Physiology II, Nara Medical University School of Medicine, Nara; and [3]Department of Artificial Organs, National Cardiovascular Center Research Institute, Osaka, Japan; and [4]Cardiovascular Research Center, Massachusetts General Hospital, Harvard Medical School, Boston, Massachusetts

Submitted 24 October 2008; accepted in final form 3 February 2009

Takewa Y, Chemaly ER, Takaki M, Liang LF, Jin H, Karakikes I, Morel C, Taenaka Y, Tatsumi E, Hajjar RJ. Mechanical work and energetic analysis of eccentric cardiac remodeling in a volume overload heart failure in rats. Am J Physiol Heart Circ Physiol 296: H1117–H1124, 2009. First published February 6, 2009; doi:10.1152/ajpheart.01120.2008.—Eccentric cardiac remodeling seen in dilated cardiomyopathy or regurgitant valvular disease is a well-known process of heart failure progression, but its mechanoenergetic profile has not been yet established. We made a volume overload (VO) heart failure model in rats and for the first time investigated left ventricular (LV) mechanical work and energetics in cross-circulated whole heart preparations. Laparotomy was performed in 14 Wistar male rats, and abdominal aortic-inferior vena caval shunt was created in seven rats (VO group). Another seven rats underwent a sham operation without functional shunt (Sham group). LV dimensions changes were followed with weekly transthoracic echocardiography. Three months after surgery, we measured LV pressure and volume and myocardial O_2 consumption in isolated heart cross circulation. LV internal dimensions in both systolic and diastolic phases were significantly increased in the VO group versus the Sham group (P 0.05). LV pressure was markedly decreased in the VO group versus in the Sham group (P 0.05). LV end-systolic pressure-volume relation shifted downward, and myocardial O_2 consumption related to Ca^2 handling significantly decreased. The contractile response to Ca^2 infusion was attenuated. Nevertheless, the increase in Ca^2 handling-related O_2 consumption per unit change in LV contractility in the VO group was significantly higher than that in the Sham group (P 0.05). The levels of sarco(endo)plasmic reticulum Ca^2 -ATPase 2a protein were reduced in the VO group (P 0.01). In conclusion, VO failing rat hearts had a character of marked contractile dysfunction accompanied with less efficient energy utilization in the Ca^2 handling processes. These results suggest that restoring Ca^2 handling in excitation-contraction coupling would improve the contractility of the myocardium after eccentric cardiac remodeling.

eccentric left ventricular hypertrophy; myocardial oxygen consumption; Ca^2 handling; sarco(endo)plasmic reticulum Ca^2 -ATPase 2a; cross circulation; aortocaval shunt

HEART FAILURE IS A MAJOR CAUSE of mortality and morbidity. It is due to various diseases such as hypertension, ischemic heart disease, valvular heart disease, congenital heart disease, cardiomyopathy, myocarditis, and others. The heart is subject to excessive and/or long-term overload, which induces myocardial hypertrophy. Hypertrophy initially compensates cardiac function but finally leads to heart failure. The process of hypertrophy and heart failure progression is divided into two mechanisms, depending on the type of overload: pressure overloading (PO) and volume overloading (VO). PO induces concentric hypertrophy to normalize wall stress from the increase in pressure placed on cardiomyocytes. Concentric remodeling of the left ventricle (LV) is characterized by an increase in ventricular wall thickness due to vertical growing of cardiomyocytes, which is caused by the parallel addition of sarcomeres (8).

Conversely, VO promotes eccentric hypertrophy to compensate for excess blood volume in the LV chamber. Eccentric remodeling of the LV is characterized by a relatively small increase in wall thickness and longitudinal growing of cardiomyocytes.

Morphological analyses, functional studies using echocardiography (4), and molecular studies (10) have been conducted on both PO and VO rat hearts. However, the cardiac mechanoenergetics studies have not yet been well conducted. We have established a method to analyze specifically the LV mechanical work and energetics in an excised, blood-perfused whole heart preparation with a cross-circulation method (7, 14, 17, 19, 20, 24) and analyzed LV mechanoenergetics in a PO heart failure model.

In the present study, we focused on the investigation of the mechanical work and energetics in a VO heart failure model with an arteriovenous (AV) shunt in rats.

MATERIALS AND METHODS

Animals

All animal experiments were performed with the approval of the Animal Care Committee of the Massachusetts General Hospital and the Mount Sinai School of Medicine and in accordance with the National Institutes of Health Guide for the Care and Use of Laboratory Animals. Fourteen male Wistar rats (Charles River, MA) weighing 300–350 g were randomized into two groups: 1) rats subjected to abdominal aortocaval shunt procedures as described previously (VO rats, n 7) (22) and 2) Sham-operated rats (Sham rats, n 7).

Creation of the Animal Models

VO was induced via the aortocaval shunt method (5, 22). All rats were anesthetized for surgery with intraperitoneal injection of 50 mg/kg pentobarbital sodium. After endotracheal intubation, artificial

Address for reprint requests and other correspondence: R. J. Hajjar, Cardiovascular Research Center, Mount Sinai School of Medicine, One Gustave Levy Place, Box 1030, New York, NY 10029 (e-mail: roger.hajjar@mssm.edu).

The costs of publication of this article were defrayed in part by the payment of page charges. The article must therefore be hereby marked "advertisement" in accordance with 18 U.S.C. Section 1734 solely to indicate this fact.

ventilation was initiated. Heparin (200 units ip) was added to prevent thrombosis during aortic and vena caval occlusion and promote shunt patency. Ventral laparotomy was performed, and the abdominal aorta and inferior vena cava were exposed by blunt dissection between the renal arterial branch and the iliac bifurcation. Both vessels were temporally occluded at both proximal and distal sites of the intended shunt point with a Bulldog clip. An 18-gauge angio-catheter was inserted over a needle into the exposed free wall of the abdominal aorta and advanced through the medial wall into the vena cava to create the shunt. After the needle and the angio-catheter were withdrawn, the ventral aortic puncture site was sealed with a drop of cyanoacrylate (Krazy Glue; Elmer's Product Canada, Toronto, Ontario, Canada) to prevent or stop bleeding from the aortic puncture site. Successful shunt could be confirmed by seeing the mixing of oxygenated blood into the vena cava from the abdominal aorta. Sham-operated animals served as controls and were subjected to the same surgeries but had no functional shunt.

Echocardiography

Cardiac function after shunt creation was monitored weekly with transthoracic echocardiography (M mode and pulse wave Doppler) using a Vivid 7 ultrasound system (GE Healthcare, Waukesha, WI) equipped with a 14-MHz transducer under sedation with a low dose (25 mg/kg ip) of pentobarbital sodium. An M-mode pacing of the LV was obtained from the parasternal short-axis view at the level of the papillary muscles. M-mode recordings were then analyzed at a sweep speed of 150 mm/s with the axis of the probe aligned with the middle of the ventricle. The following parameters were measured and calculated using the leading edge method described by the American Society of Echocardiography (4, 12): LV internal dimensions (LVID) at both diastole and systole (LVIDd and LVIDs, respectively), LV posterior wall dimensions at both diastole and systole, interventricular septal (IVS) dimensions at both diastole (IVSd) and systole, heart rate (HR), percentage of LV fractional shortening, LV ejection fraction (EF), and cardiac output.

LV Mechanical and Energetic Studies

Surgical preparations. LV mechanical and energetic studies were performed 3 mo after the creation of aortocaval shunt on the excised cross-circulated rat heart preparations, as reported previously (13). In each experiment, one VO or Sham rat and two retired breeder male crj:Wistar rats weighing 450–650 g were anesthetized with pentobarbital sodium (50 mg/kg ip), intubated, and ventilated. The study rat (VO or Sham) was used as heart donor, and the other two were used as blood supplier and metabolic supporter rats, respectively. All rats were heparinized (1,000 units intravascular). The beating donor heart was excised without an interruption of coronary perfusion and supported by cross circulation with the other metabolic supporter rat as previously reported in detail (7, 14, 17, 19, 24). The coronary arterial oxygenated blood of the donor heart was supplied from the common carotid arteries of the supporter rat using arterial cross-circulation tubing and a cannula inserted into the brachiocephalic artery of the donor heart. The coronary venous blood of the donor heart was collected from a cannula inserted into the right ventricle (RV) via the superior vena cava and the right atrium and returned to the right external jugular vein of the supporter rat using venous cross-circulation tubing and a cannula. The excised heart was maintained at 37°C by a heater. A thin latex balloon (balloon material volume, 0.08 or 0.10 ml) was inserted from the left atrial appendage into the LV and primed with water. The maximum unstretched volume of the used balloon was large enough to exceed measured end-diastolic volume in both VO and Sham rat hearts. The balloon was connected to a 0.5-ml precision glass syringe with fine scales (minimum scale, 0.005 ml) to allow changing LV volume (LVV) in 0.025-ml steps and also connected to a pressure transducer for measuring LV pressure (LVP) measurement. LVV was increased in steps up to an end-diastolic pressure (EDP) of around 10 mmHg in the control volume run. Systolic unstressed volume (V_0) was determined by filling the balloon to the level where peak isovolumic pressure and hence pressure-volume area (PVA; see Data Analysis) were zero. The sum of intraballoon water volume and balloon material volume was used as an initial estimate of V_0. V_0 normalized by LV mass to 1 g was then finally determined as the volume-axis intercept of the best-fit end-systolic pressure (ESP)-volume relation (ESPVR). We obtained the best-fit ESPVR with an equation (ESP A{1 exp[B(V V_0)]}; A and B are parameters) by means of the least-squares method (DeltaGraph, DeltaPoint; Monterey, CA) on a personal computer (14, 17, 19, 24). We also obtained the best-fit EDP-volume relation (EDPVR) with an equation (EDP A {exp[B (V V_0)] 1}; A and B are parameters). Correlation coefficients of the best-fit ESPVRs were higher than 0.98 (Table 1).

The HR was constantly maintained by electrical pacing of the right atrium, and the pacing rate was adjusted around 300 beats/min to avoid causing incomplete relaxation or arrhythmia. The systemic arterial blood pressure of the supporter rat served as the coronary perfusion pressure (90–120 mmHg). Arterial O_2 saturation and O_2 content of the supporter rat were monitored with an oximeter (model IL682 CO-Oxymeter; Instrumentation Laboratory) and maintained within their physiological ranges with ventilation adjustment and supplemental O_2 and sodium bicarbonate.

Calculation of O_2 consumption. Total myocardial O_2 consumption per beat ($\dot{V}O_2$) was obtained as the product of coronary flow and coronary AV O_2 content difference (AVO_2D) divided by the pacing rate (300 beats/min) (14, 17, 19, 24). Total coronary blood flow was continuously measured with an ultrasonic flowmeter (model T206; Transonic System, Ithaca, NY) placed in the middle of the venous drainage tubing from the RV. LV thebesian flow is negligible. The coronary AVO_2D was continuously measured by passing all the arterial and venous cross-circulation blood through the cuvettes of a custom-made AVO_2D analyzer (PWA-200S, Shoe Technica; Chiba, Japan) as previously reported in detail (14, 17, 19, 24).

Calculation of PVA. PVA was defined as the systolic PVA circumscribed by the curvilinear ESPVR, the EDPVR, and the systolic portion of the ventricular pressure-volume trajectory and was obtained by the integration of ESPVR and EDPVR. The areas under the ESPVR and EDPVR were obtained by the integration of the best-fit exponential functions. Based on our previous publications (14, 17, 19, 24), we obtained control ESPVR and determined a midrange LV volume (mLVV) under which contractility changes in response to Ca^2 infusion (16). As the balloon volume generally changed between 0 and 0.10 ml in Sham rats and between 0 and 0.20 ml in VO rats, respectively, we adopted mLVV normalized by LV mass to 1 g at balloon volume of 0.05 ml for Sham LVs and at balloon volume of 0.10 ml for VO LVs. We calculated ESP at mLVV (ESP_{mLVV}) and PVA at mLVV (PVA_{mLVV}) to assess LV mechanical work and energetics in the two groups.

As shown previously (14, 17, 19, 24), the $\dot{V}O_2$-PVA relationship was linear in the rat LV. Its slope represents the O_2 cost of PVA, and

Table 1. Variables of bodies, hearts, and lungs

	Sham		VO		P
Body weight, g	609	81	609	66	0.823
LV weight, g	1.05	0.15	1.41	0.21	0.016*
RV weight, g	0.23	0.04	0.38	0.07	0.006*
LV RV weight, g	1.28	0.18	1.79	0.26	0.008*
LV weight/body weight, %	0.17	0.02	0.23	0.02	0.007*
RV weight/body weight, %	0.03	0.01	0.06	0.01	0.005*
LV RV weight/body weight, %	0.21	0.02	0.29	0.03	0.004*
Lung weight, g	1.97	0.47	2.26	0.48	0.319

Values are means SD; n 7 Sham rats and 7 volume overload (VO) rats. LV, left ventricle; RV, right ventricle; P, value of probability. *P 0.05 vs. Sham.

its $\dot{V}O_2$ intercept represents the PVA-independent $\dot{V}O_2$. The PVA-independent $\dot{V}O_2$ is composed of $\dot{V}O_2$ in excitation-contraction (E-C) coupling (18) and basal metabolism (11, 17). The RV was kept collapsed (and therefore unloaded) by continuous hydrostatic drainage of the coronary venous return so that the RV PVA and hence PVA-dependent $\dot{V}O_2$ were assumed to be negligible (19, 20). The RV component of total $\dot{V}O_2$, which is considered constant irrespective of LV volume, was calculated by multiplying biventricular $\dot{V}O_2$ under unloaded LV volume with the ratio of the RV weight divided by the sum of the RV and LV weight. The RV PVA-independent $\dot{V}O_2$ (14, 17, 19, 24) was subtracted from the total $\dot{V}O_2$ to yield LV $\dot{V}O_2$ expressed as $\dot{V}O_2$. The LV (including the septum) and the RV were weighed at the end of the experiment for normalization of LVV.

Experimental protocol. LVP, LV $\dot{V}O_2$, and systolic PVA data were obtained at more than five different LV volumes from 0 to 0.2 ml of intraballoon volume in 0.025-ml increments, without inotropic interventions [control volume-loading run (vol-run)]. After the vol-run, the Ca^2 inotropic run (Ca^2 ino-run) was performed at an mLVV by intracoronary infusion of 1% $CaCl_2$ solution. The infusion rate of $CaCl_2$ solution was increased stepwise from 0 to 6 ml/h. Steady-state $\dot{V}O_2$ was reached 2 to 3 min after change of LV volume and 4 min after change of infusion rate. Finally, cardiac arrest was induced by intracoronary infusion of 1 M KCl (12 ml/h) to obtain O_2 consumption for basal metabolism. At each steady state, data were sampled at 500 Hz for 2 s simultaneously, and the sampling was usually repeated three times at 0.5- to 1-min intervals.

Data Analysis

$\dot{V}O_2$ for Ca^2 handling during the Ca^2 ino-run. In previous mechanoenergetic studies in excised rat hearts (14, 17, 19, 24), a linear $\dot{V}O_2$-PVA relation obtained during Ca^2 infusion (Ca^2 $\dot{V}O_2$-PVA relation) was shifted upward in parallel with the control $\dot{V}O_2$-PVA relation before Ca^2 infusion. Such parallelism was also observed in VO rat hearts in our preliminary experiments. The $\dot{V}O_2$-intercept (PVA-independent $\dot{V}O_2$) corresponds primarily to the $\dot{V}O_2$ for Ca^2 handling in E-C coupling and for basal metabolism (11, 17, 18). The increased $\dot{V}O_2$ intercept of the Ca^2 $\dot{V}O_2$-PVA relation is attributable to the increased $\dot{V}O_2$ for enhanced Ca^2 handling due to the unchanged $\dot{V}O_2$ for basal metabolism (17). Thus, at increasing levels of inotropy, the intercept of the $\dot{V}O_2$-PVA relationship increases, but the slope remains unchanged. Based on this parallelism, the lines of $\dot{V}O_2$-PVA linear relationships at different rates of Ca^2 infusion at an mLVV were drawn in parallel to the control $\dot{V}O_2$-PVA relation line, as described previously (14, 17, 19, 24).

During the Ca^2 ino-run at an mLVV, ESPVR curves at different infusion rates were obtained as best-fit exponential function curves. We calculated PVA_{mLVV} during Ca^2 infusion on a personal computer (14, 17, 19, 24). We then obtained the two composite $\dot{V}O_2$-PVA_{mLVV} data points. After we drew the lines, including each $\dot{V}O_2$-PVA_{mLVV} data point, in parallel to the control $\dot{V}O_2$-PVA relation, we obtained the $\dot{V}O_2$ intercept at each infusion rate. We subtracted basal metabolic $\dot{V}O_2$ per beat, measured in KCl-arrested hearts, from PVA-independent $\dot{V}O_2$ to obtain $\dot{V}O_2$ for Ca^2 handling in E-C coupling.

LV contractility. Our recently proposed index for LV contractility (i.e., equivalent maximal elastance [eE_{max}]) was calculated from ESP-volume ratio of the specific virtual triangular area, which is energetically equivalent to PVA_{mLVV} as previously described (17, 20).

O_2 cost of LV contractility. The O_2 cost of LV contractility was obtained as the slope of the linear relation between $\dot{V}O_2$ for Ca^2 handling in E-C coupling and eE_{max} at an mLVV during the Ca^2 ino-run. At every infusion rate, there was a corresponding eE_{max} and a corresponding $\dot{V}O_2$ for Ca^2 handling in E-C coupling derived from the $\dot{V}O_2$-PVA intercept (PVA-independent $\dot{V}O_2$). eE_{max} and PVA-independent $\dot{V}O_2$ were also linearly related. The slope of the latter linear relationship, defined as the O_2 cost of LV contractility, quantifies the change in $\dot{V}O_2$ for Ca^2 handling per unit change in LV contractility.

Western blot for sarco(endo)plasmic reticulum Ca^2 -ATPase 2a and sodium-calcium exchanger proteins. LV myocardium from each heart was frozen and stored at 80°C after the mechanoenergetic studies. The frozen hearts were thawed and homogenized. The homogenates were matched for protein concentration, subjected to SDS-PAGE, and transferred to nitrocellulose membranes. For immunoreactions, the blots were incubated with primary antibodies to sarco(endo)plasmic reticulum Ca^2 -ATPase 2a (SERCA2a; Affinity Bioreagents, Golden, CO), sodium-calcium exchanger (NCX)1 [Chemicon (Millipore), Billerica, MA], and GAPDH (Sigma-Aldrich, St. Louis, MO) and then subjected to enhanced chemiluminescence for detection. Both SERCA2a and NCX1 expressions were normalized to GAPDH expression.

Statistical analysis. Values are means SD. Comparison of paired and unpaired individual values was performed by the paired and unpaired t-test, respectively. A value of P 0.05 was considered statistically significant. All data are expressed as the means SD.

RESULTS

Echocardiography

Typical M-mode echocardiograms in both VO and sham rats 10 wk after operation are displayed in Fig. 1.

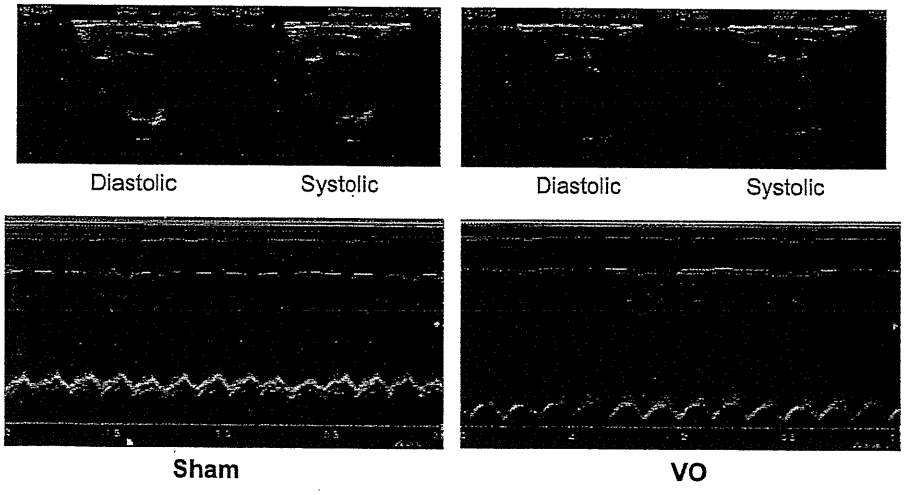

Fig. 1. Representative M-mode echocardiograms in both volume overloading (VO) and Sham rats 10 wk after aortocaval shunt creation. Left ventricular (LV) internal dimensions at both diastole and systole (LVIDd and LVIDs, respectively) were markedly increased in VO rats compared with those in Sham rats.

Figure 2 demonstrates serial changes in mean values of the LVIDd, LVIDs, EF, and IVS. From as early as 2 wk postsurgery, LVIDd significantly increased in VO compared with Sham rats. This trend continued up to 12 wk where VO rats exhibited chamber dilatation at diastole that reached 140% of that in Sham rats. The LVIDs in the VO group was significantly increased from 3 wk after shunt compared with that in the Sham group, then continued to increase gradually, and reached 150% of that in Sham rats after 9 wk. The delay means that the decreasing of cardiac contractility became notable 3 wk after shunt and took at least 9 wk to get worst. The EF in the VO group was increased for the first 2 wk after AV shunt creation and then decreased gradually, and the reduction less than Sham group was first noted at 6 wk. The IVSd in the VO group was slightly thinner compared with that in the Sham group.

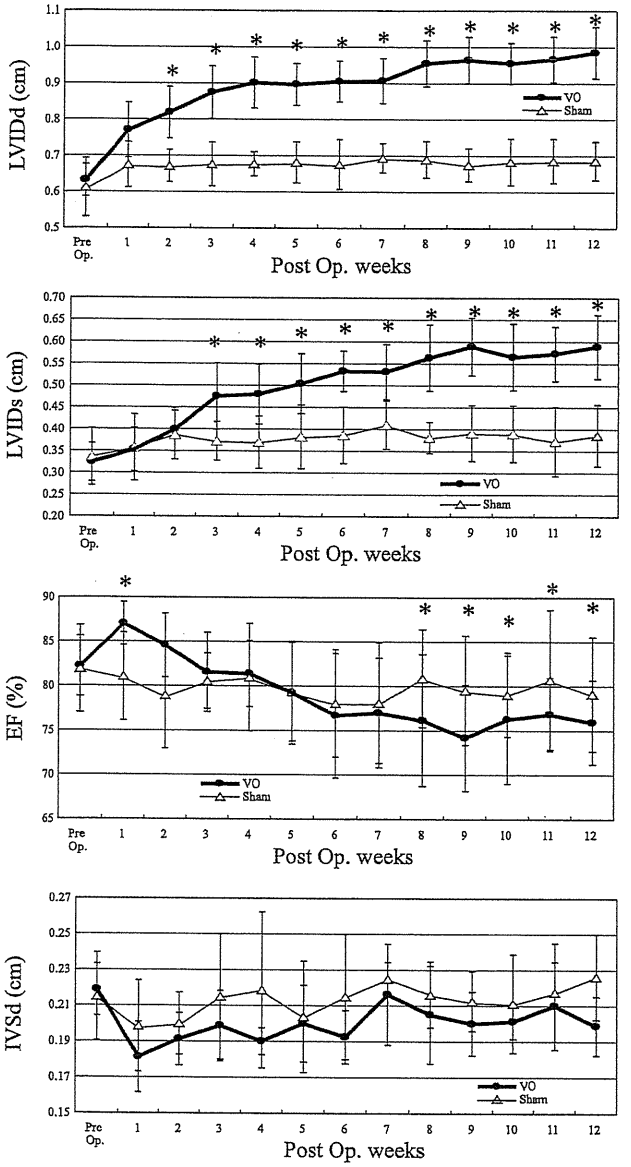

Fig. 2. Serial changes in echocardiographic parameters in VO and Sham rats. The LVIDd, LVIDs, percentage of LV ejection fraction (EF), percentage of LV fractional shortening, and interventricular septal dimensions in diastole (IVSd) are shown. *P 0.05 vs. Sham. As early as 2 wk after the surgery, LVIDd significantly increased in VO compared with Sham rats. This trend continued up to 12 wk where VO rats exhibited chamber dilatation in diastole that reached 140% of that in Sham rats. The LVIDs in the VO group was significantly increased from 3 wk after shunt compared with that in the Sham group, then continued to increase gradually, and reached 150% of that in Sham rats after 9 wk. The EF in the VO group was increased at first 2 wk after arteriovenous shunt but then decreased gradually to become less than Sham group at 6 wk. The IVSd in the VO group was slightly thinner compared with that in the Sham group. Post Op, postoperation of shunt creation or sham procedure.

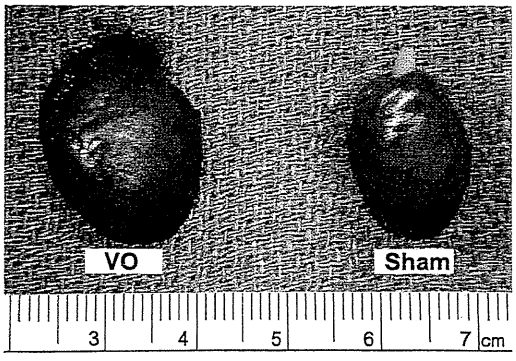

Fig. 3. Whole hearts 3 mo after aortocaval shunt surgery in both VO and Sham rats. The heart in the VO group was markedly enlarged compared with that in the Sham group.

Characterization of Hearts and Lungs

Figure 3 demonstrates the pictures of whole ventricle 3-mo post surgery. The heart in the VO group was remarkably

Table 2. Variables of LV mechanical works and energetics

	Sham		VO		P
ESPVR					
A, mmHg	195	35	134	23	0.003*
B, 1/ml	31.8	24.5	31.6	16.3	0.911
V_0, 10 ^{2} ml/g of LV	7.79	1.11	7.36	1.37	0.601
EDPVR					
A , mmHg	0.20	0.34	0.30	0.26	0.483
B , 1/ml	23.2	9.3	17.1	4.7	0.301
ESP_{mLVV}, mmHg					
Pre-Ca^2 infusion	130	39	98	19	0.039*
Under Ca^2 infusion, 1% $CaCl_2$ 6 ml/h	186	37	127	24	0.003*
ESP_{mLVV}	56	30	29	25	0.045*
$eE_{max,mLVV}$ (baseline), mmHg ml ^{1} g	3,760	1,580	2,395	1,171	0.040*
$\dot{V}O_2$-PVA relation					
Slope, 10 ^{3} l O_2 mmHg ^{1} ml ^{1}	9.70	2.90	7.46	2.63	0.372
$\dot{V}O_2$ intercept, 10 ^{1} l O_2 beat ^{1} g ^{1}	2.77	0.70	2.06	0.89	0.040*
Basal metabolism, l O_2 min ^{1} g ^{1}	16.8	5.9	15.4	4.7	0.123
PVA-independent $\dot{V}O_2$-$eE_{max,mLVV}$ relation					
Slope, O_2 cost of LV contractility, 10 ^{5} l O_2 ml mmHg ^{1} beat ^{1} g ^{2}	6.12	2.14	20.37	6.68	0.047*

Values are means SD; n 7 Sham rats and 7 VO rats. ESPVR, end-systolic pressure-volume relation; EDPVR, end-diastolic pressure-volume relation; ESP_{mLVV}, end-systolic pressure at midrange LV volume (mLVV; see Calculation of PVA); ESP_{mLVV}, (ESP_{mLVV} under Ca^2 infusion) (ESP_{mLVV} pre-Ca^2 infusion); $eE_{max,mLVV}$, equivalent maximal elastance at mLVV; $\dot{V}O_2$, myocardial oxygen consumption per beat; PVA, pressure-volume area. See LV Mechanical and Energetic Studies for ESPVR and EDPVR parameters. V_0 is the unstressed LV volume normalized by LV mass to 1 g. *P 0.05 vs. Sham.

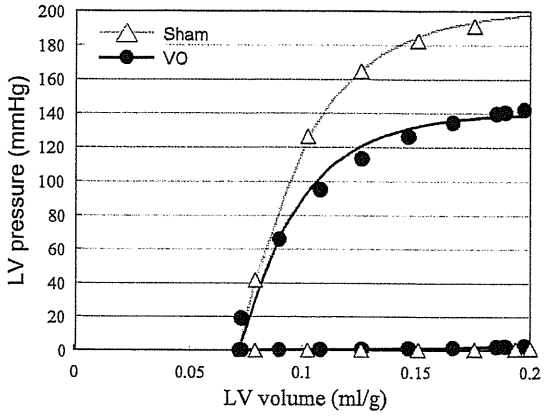

Fig. 4. Representative LV pressure-volume data and the best-fit curves [LV end-systolic pressure (ESP)-volume relation (ESPVR), LV end-diastolic pressure-volume relation (EDPVR)] in each heart for both VO and Sham groups. The LV ESP was markedly decreased in the VO compared with the Sham heart. The LV ESPVR shifted downward but the EDPVR did not shift upward in the VO heart.

enlarged compared with that in the Sham group. Both the LV and RV weights in the VO group were significantly heavier than those in the Sham group (Table 1).

LV Contractility

Summarized data of LV mechanical work and energetics are shown in Table 2.

Figure 4 shows a representative data and best-fit curves of the ESPVR and EDPVR in both VO and Sham group. The LV ESPVR shifted downward, and thus the mean LV ESP_{mLVV} was significantly decreased in the VO group compared with the Sham group (P 0.01; Table 2), although the EDPVR did not shift upward.

Figure 5 shows representative data and best-fit ESPVRs during the Ca^2 infusion of both VO and Sham groups. The contractile response to Ca^2 infusion at a given concentration was smaller in the VO group than that in the Sham group. The mean ESP_{mLVV} in the VO group was significantly smaller (P 0.05) than that in Sham group (Table 2).

LV Energetics

Summarized data of LV energetics are also shown in Table 2.

$\dot{V}O_2$-PVA Relationship

Figure 6 shows each set of representative $\dot{V}O_2$-PVA data and the best-fit $\dot{V}O_2$-PVA linear relations in VO and Sham hearts. The $\dot{V}O_2$ intercept was smaller in this VO heart than in the Sham heart, but the slopes of both $\dot{V}O_2$-PVA relations were similar. The mean $\dot{V}O_2$ intercept was significantly smaller in the VO group than that in the Sham group (Table 2), but the mean slopes of $\dot{V}O_2$-PVA linear relations did not differ significantly between VO and Sham groups (Table 2). Basal metabolism obtained by KCl arrest was unchanged in the VO and Sham groups (Table 2) and thus the significantly smaller $\dot{V}O_2$ intercept in VO group was due to the decreased O_2 consumption associated with Ca^2 handling in E-C coupling.

O_2 Cost of LV Contractility

Figure 7 shows each set of representative PVA-independent $\dot{V}O_2$-$eE_{max,mLVV}$ data and best-fit PVA-independent $\dot{V}O_2$-$eE_{max,mLVV}$ regression lines in both VO and Sham hearts. Each slope of the regression lines denotes the O_2 cost of LV contractility, an index quantifying the $\dot{V}O_2$ for Ca^2 handling per unit change in LV contractility, as mentioned in Data Analysis. The O_2 cost of LV contractility in this VO heart was higher than that in the Sham heart. The mean O_2 cost of LV contractility in the VO group was significantly higher (P 0.05) than that in the Sham group (Table 2).

Immunoblotting of SERCA2a and NCX Normalized to GAPDH

The mean protein level of SERCA2a in VO rat hearts was significantly lower (P 0.01) than that in Sham rat hearts (Fig. 8). We also observed elevated levels (P 0.01) of NCX protein in VO rat hearts (Fig. 9).

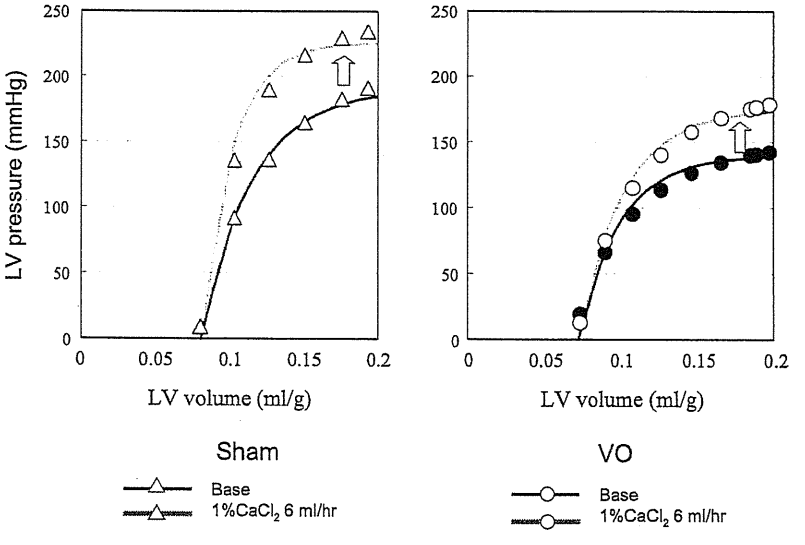

Fig. 5. Representative LV pressure-volume data and ESPVRs under Ca^2 infusion at a rate of 6 ml/h in both hearts from Sham and VO groups. The contractile response to Ca^2 infusion was smaller in the VO heart than that in the Sham heart.

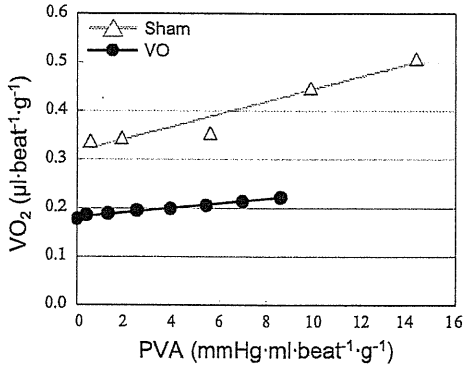

Fig. 6. Representative $\dot{V}O_2$-pressure-volume area (PVA) data and best-fit linear regression lines (the $\dot{V}O_2$-PVA linear relations). The $\dot{V}O_2$ intercept was smaller in the VO heart than in the Sham heart, but the slopes were similar in both VO and Sham hearts.

DISCUSSION

There were several major findings in the VO rats in the present study. LV ESPVR shifted downward, and thus mean ESP_{mLVV} and mean $eE_{max,mLVV}$ (at an mLVV) were significantly decreased compared with those in the Sham rats, indicating systolic dysfunction. The contractile response to Ca^2 infusion (ESP_{mLVV}) was significantly smaller in the VO rats than in the Sham rats. The mean slope of the $\dot{V}O_2$-PVA relation was hardly changed, but the $\dot{V}O_2$ intercept was significantly decreased with unchanged basal metabolism compared with those in the Sham rat, indicating the decreased Ca^2 handling-related $\dot{V}O_2$ at baseline. Finally, the mean slope of the relationship between Ca^2 handling-related $\dot{V}O_2$ and eE_{max} was significantly increased, indicating a less efficient energy utilization in the Ca^2 handling process.

Mechanical Function after AV Shunt

The VO rats created in the present study mainly showed LV systolic dysfunction, whereas diastolic function was almost unchanged. This is compatible with previous studies in a similar VO model in which LV eccentric hypertrophy and systolic dysfunction were apparent, whereas diastolic function and compliance of the ventricle were unchanged or enhanced

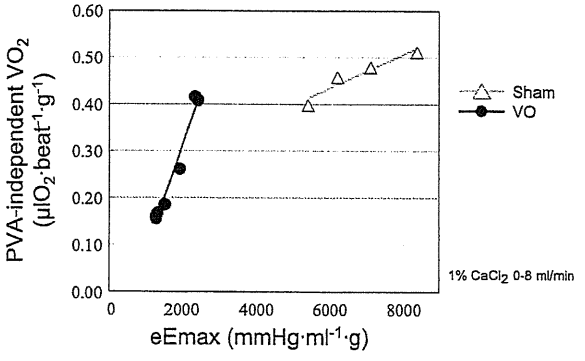

Fig. 7. Representative PVA-independent $\dot{V}O_2$-equivalent maximal elastance (eE_{max}) midrange LV volume data and best-fit regression line (the PVA-independent $\dot{V}O_2$-eE_{max} linear relation; the slope of the relation is the O_2 cost of LV contractility). The O_2 cost of LV contractility in this VO heart was higher than that in the Sham heart.

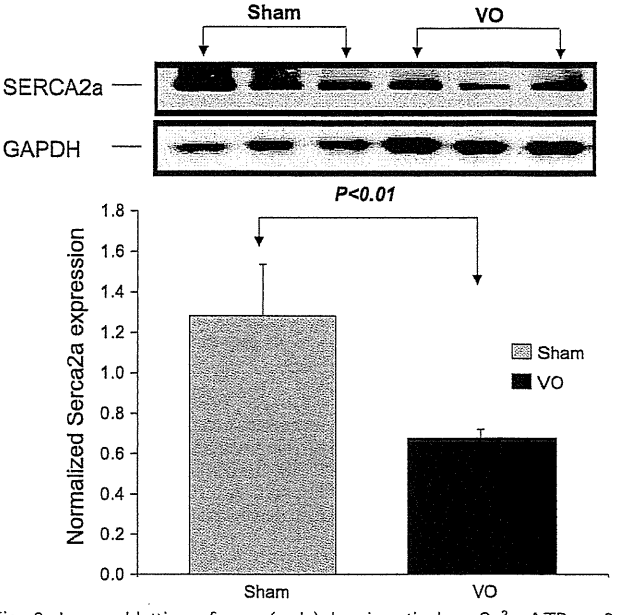

Fig. 8. Immunoblotting of sarco(endo)plasmic reticulum Ca^2 -ATPase 2a (SERCA2a) normalized to GAPDH. The mean protein level of SERCA2a in VO rat hearts was significantly lower (P 0.01) than that in Sham rat hearts.

(4). It is generally accepted that derangement of intracellular Ca^2 handling can play a crucial role in the development of the systolic and diastolic dysfunction accompanying arrhythmia. The mechanism of the LV contractile dysfunction in the present study can be also explained by a derangement of the Ca^2 handling process involved in E-C coupling.

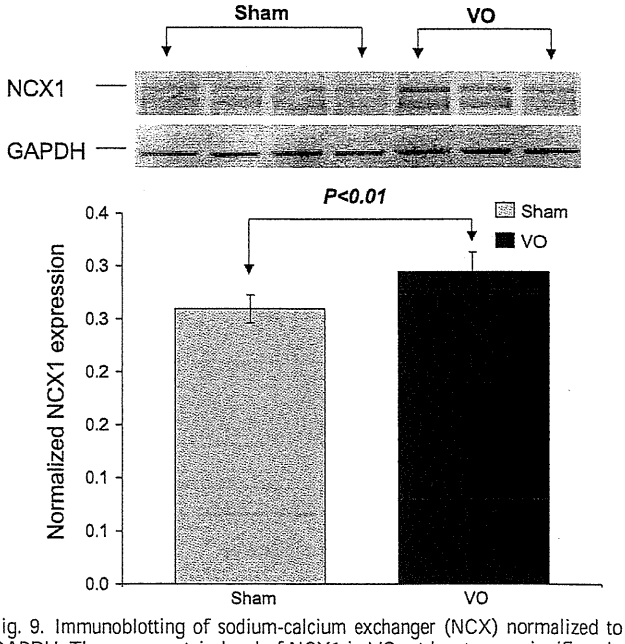

Fig. 9. Immunoblotting of sodium-calcium exchanger (NCX) normalized to GAPDH. The mean protein level of NCX1 in VO rat hearts was significantly higher than that in Sham rat hearts.

Ca^2 Handling in E-C Coupling

We have previously reported that Ca^2 overload in the cytoplasm due to the impairment of the total Ca^2 handling in E-C coupling in the myocardium induced acute cardiac failure (19). The total Ca^2 handling in the myocardium is regulated by transsarcolemmal Ca^2 influx via L-type Ca^2 channel, Ca^2 -induced Ca^2 release via the ryanodine receptor, Ca^2 uptake via the SERCA2a pump, NCX, and Na -K pump coupled to NCX (17). The decreased activity of SERCA2a reduces Ca^2 uptake to the sarcoplasmic reticulum, leading to an increase in cytosolic Ca^2 in diastole and a reduction in Ca^2 release in systole.

In the VO rat, the LV $\dot{V}o_2$-PVA relation has a lower intercept with almost unchanged slope, indicating that total Ca^2 handling O_2 consumption in E-C coupling is decreased under baseline conditions. However, the LV contractility-Ca^2 handling O_2 consumption has a higher slope (O_2 cost of LV contractility), suggesting one possibility that Ca^2 uptake via the SERCA2a pump is suppressed and instead NCX activity is enhanced during inotropic stimulation. Although NCX per se does not consume ATP to remove cytosolic Ca^2 in exchange with influx Na (stoichiometry of 3Na :1Ca^2), the influx Na must be pumped out by Na -K -ATPase with a stoichiometry of 3Na :2K :1ATP, resulting in the net stoichiometry of 1Ca^2 :1ATP (3). On the other hand, SERCA2a removes cytosolic Ca^2 on the basis of a stoichiometry of 2Ca^2 :1ATP. Therefore, the Ca^2 extrusion via NCX leads to twice the increase in energy expenditure compared with Ca^2 uptake by SERCA2a. Thus it seems most likely that the energy wasting in Ca^2 handling is induced mainly by the enhanced NCX activity. In the present study, the expression of the NCX protein was increased in the VO LV tissue. We also reported the same kinds of increased O_2 consumption related to increased NCX activity in a PO hypertrophied rat heart (15). In the failing human heart, a reduction in SERCA2a expression and an increase in NCX expression have been reported (2, 9). This theory was supported by the result in the present study that the SERCA2a protein level was decreased and the NCX protein level was elevated in VO rat hearts. Therefore, in the VO rats, decreased Ca^2 uptake via the SERCA2a pump has impaired cardiac contractility and simultaneously induced energy wasting in E-C coupling.

Another possibility for higher O_2 cost of LV contractility is due to leaky ryanodine receptors. Leaky ryanodine receptors can cause higher cytosolic Ca^2 concentrations in diastole (23), suggesting the possibility for increased energy expenditure by SERCA2a pump. However, the latter hypothesis is unlikely to explain all our findings; indeed, the protein level of SERCA2a in the VO rat hearts was lower than that in the Sham rat hearts, unless NCX1 is upregulated.

A third possibility is due to a lower Ca^2 sensitivity of the myofilament, since ESP_{mLVV} induced by Ca^2 infusion was significantly smaller in the VO rat hearts (see Table 2). However, the increase of PVA-independent $\dot{V}o_2$ was actually larger in the VO rat heart than that in the Sham rat heart under the same protocol for Ca^2 infusion (see Fig. 7). Therefore, the higher O_2 cost of LV contractility seems rather to derive from the larger increase of PVA-independent $\dot{V}o_2$.

Taken together, the possibility that Ca^2 uptake via the SERCA2a pump is suppressed and instead NCX activity is enhanced is the most likely explanation for our findings (15), although further studies including SERCA2a overexpression by gene transfer are needed to verify this possibility.

Chemomechanical Energy Transduction

In the VO hearts, the slope of the $\dot{V}o_2$-PVA relation was almost unchanged or slightly lower compared with that of the Sham heart. The slope of the $\dot{V}o_2$-PVA relation remained unchanged in hypothyroid (11) and diabetic (1) rat hearts, whereas a steeper slope of the $\dot{V}o_2$-PVA relation was reported in hyperthyroid rabbit hearts. It was reported that the slope of the $\dot{V}o_2$-PVA relation was related to the ratio of the myosin isoform component from predominantly V3 to predominantly V1 (i.e., the slope of the $\dot{V}o_2$-PVA relation increases when the V1-to-V3 ratio increases, and the slope of the $\dot{V}o_2$-PVA relation is unchanged when the V1-to-V3 ratio decreases) (6). It was also reported that a progressive decrease in V1 and an increase in V3 were apparent in the LV 8- to 16 wk after AV shunt (21). This report is consistent with the almost unchanged slope of the $\dot{V}o_2$-PVA relation in the VO rats. The slope of $\dot{V}o_2$-PVA relation reflects the ratio of chemomechanical energy transduction efficiency of the contractile machinery. Therefore, in the VO rats, energy wasting is not related to chemomechanical energy transduction.

Conclusion

VO failing rat hearts had a character of marked contractile dysfunction accompanied with inefficient energy utilization especially in E-C coupling.

Present results suggest that restoring the Ca^2 handling process in E-C coupling would improve myocardial contractility in the setting of eccentric cardiac remodeling.

GRANTS

This work was supported in part by National Heart, Lung, and Blood Institute Grants RO1-HL-078691, HL-071763, HL-080498, and HL-083156 (to R. Hajjar) and a grant from Transatlantic Network.

REFERENCES

1. **Abe T, Ohga Y, Tabayashi N, Kobayashi S, Sakata S, Misawa H, Tsuji T, Kohzuki H, Suga H, Taniguchi S, Takaki M.** Left ventricular diastolic dysfunction in type 2 diabetes mellitus model rats. Am J Physiol Heart Circ Physiol 282: H138–H148, 2002.
2. **Arai M, Matsui H, Periasamy M.** Sarcoplasmic reticulum gene expression in cardiac hypertrophy and heart failure. Circ Res 74: 555–564, 1994.
3. **Bers DM.** Calcium fluxes involved in control of cardiac myocyte contraction. Circ Res 87: 275–281, 2000.
4. **Cantor EJ, Babick AP, Vasanji Z, Dhalla NS, Netticadan T.** A comparative serial echocardiographic analysis of cardiac structure and function in rats subjected to pressure or volume overload. J Mol Cell Cardiol 38: 777–786, 2005.
5. **Garcia R, Diebold S.** Simple, rapid, and effective method of producing aortocaval shunts in the rat. Cardiovasc Res 24: 430–432, 1990.
6. **Goto Y, Slinker BK, LeWinter MM.** Decreased contractile efficiency and increased nonmechanical energy cost in hyperthyroid rabbit heart. Relation between O_2 consumption and systolic pressure-volume area or force-time integral. Circ Res 66: 999–1011, 1990.
7. **Hata Y, Sakamoto T, Hosogi S, Ohe T, Suga H, Takaki M.** Linear O_2 use-pressure-volume area relation from curved end-systolic pressure-volume relation of the blood-perfused rat left ventricle. Jpn J Physiol 48: 197–204, 1998.
8. **Lorell BH, Carabello BA.** Left ventricular hypertrophy: pathogenesis, detection, and prognosis. Circulation 102: 470–479, 2000.
9. **Mercadier JJ, Lompre AM, Duc P, Boheler KR, Fraysse JB, Wisnewsky C, Allen PD, Komajda M, Schwartz K.** Altered sarcoplas-

mic reticulum Ca^2 -ATPase gene expression in the human ventricle during end-stage heart failure. J Clin Invest 85: 305–309, 1990.

10. **Miyazaki H, Oka N, Koga A, Ohmura H, Ueda T, Imaizumi T.** Comparison of gene expression profiling in pressure and volume overload-induced myocardial hypertrophies in rats. Hypertens Res 29: 1029–1045, 2006.
11. **Ohga Y, Sakata S, Takenaka C, Abe T, Tsuji T, Taniguchi S, Takaki M.** Cardiac dysfunction in terms of left ventricular mechanical work and energetics in hypothyroid rats. Am J Physiol Heart Circ Physiol 283: H631–H641, 2002.
12. **Sahn DJ, DeMaria A, Kisslo J, Weyman A.** Recommendations regarding quantitation in M-mode echocardiography: results of a survey of echocardiographic measurements. Circulation 58: 1072–1083, 1978.
13. **Sakata S, Lebeche D, Sakata N, Sakata Y, Chemaly ER, Liang LF, Takewa Y, Jeong D, Park WJ, Kawase Y, Hajjar RJ.** Targeted gene transfer increases contractility and decreases oxygen cost of contractility in normal rat hearts. Am J Physiol Heart Circ Physiol 292: H2356–H2363, 2007.
14. **Sakata S, Lebeche D, Sakata N, Sakata Y, Chemaly ER, Liang LF, Tsuji T, Takewa Y, del Monte F, Peluso R, Zsebo K, Jeong D, Park WJ, Kawase Y, Hajjar RJ.** Restoration of mechanical and energetic function in failing aortic-banded rat hearts by gene transfer of calcium cycling proteins. J Mol Cell Cardiol 42: 852–861, 2007.
15. **Shimizu J, Yamashita D, Misawa H, Tohne K, Matsuoka S, Kim B, Takeuchi A, Nakajima-Takenaka C, Takaki MT.** Increased O_2 consumption in excitation-contraction coupling in hypertrophied rat heart slices related to increased Na -Ca^2 exchange activity. Jpn J Physiol 59: 63–74, 2009.
16. **Stromer H, Cittadini A, Szymanska G, Apstein CS, Morgan JP.** Validation of different methods to compare isovolumic cardiac function in isolated hearts of varying sizes. Am J Physiol Heart Circ Physiol 272: H501–H510, 1997.
17. **Takaki M.** Left ventricular mechanoenergetics in small animals. Jpn J Physiol 54: 175–207, 2004.
18. **Takaki M, Kohzuki H, Kawatani Y, Yoshida A, Ishidate H, Suga H.** Sarcoplasmic reticulum Ca^2 pump blockade decreases O_2 use of unloaded contracting rat heart slices: thapsigargin and cyclopiazonic acid. J Mol Cell Cardiol 30: 649–659, 1998.
19. **Tsuji T, Ohga Y, Yoshikawa Y, Sakata S, Abe T, Tabayashi N, Kobayashi S, Kohzuki H, Yoshida KI, Suga H, Kitamura S, Taniguchi S, Takaki M.** Rat cardiac contractile dysfunction induced by Ca^2 overload: possible link to the proteolysis of -fodrin. Am J Physiol Heart Circ Physiol 281: H1286–H1294, 2001.
20. **Tsuji T, Ohga Y, Yoshikawa Y, Sakata S, Kohzuki H, Misawa H, Abe T, Tabayashi N, Kobayashi S, Kitamura S, Taniguchi S, Suga H, Takaki M.** New index for oxygen cost of contractility from curved end-systolic pressure-volume relations in cross-circulated rat hearts. Jpn J Physiol 49: 513–520, 1999.
21. **Wang X, Ren B, Liu S, Sentex E, Tappia PS, Dhalla NS.** Characterization of cardiac hypertrophy and heart failure due to volume overload in the rat. J Appl Physiol 94: 752–763, 2003.
22. **Wang X, Sentex E, Saini HK, Chapman D, Dhalla NS.** Upregulation of -adrenergic receptors in heart failure due to volume overload. Am J Physiol Heart Circ Physiol 289: H151–H159, 2005.
23. **Yano M, Ono K, Ohkusa T, Suetsugu M, Kohno M, Hisaoka T, Kobayashi S, Hisamatsu Y, Yamamoto T, Kohno M, Noguchi N, Takasawa S, Okamoto H, Matsuzaki M.** Altered stoichiometry of FKBP12.6 versus ryanodine receptor as a cause of abnormal Ca^2 leak through ryanodine receptor in heart failure. Circulation 102: 2131–2136, 2000.
24. **Yoshikawa Y, Hagihara H, Ohga Y, Nakajima-Takenaka C, Murata KY, Taniguchi S, Takaki M.** Calpain inhibitor-1 protects the rat heart from ischemia-reperfusion injury: analysis by mechanical work and energetics. Am J Physiol Heart Circ Physiol 288: H1690–H1698, 2005.

137　二段インペラを用いた心肺補助用血液ポンプの開発

Development of a Centrifugal Pump with the Two-stage Impeller for Cardiopulmonary Support System

○正　築谷 朋典 (国循研)　堀口 祐憲 (阪大基礎工)　辻本 良信 (阪大基礎工)
巽 英介 (国循研)　妙中 義之 (国循研)

Tomonori TSUKIYA, National Cardiovascular Center, 5-7-1, Fujishiro-dai, Suita, Osaka
Hironori HORIGUCHI, Yoshinobu TSUJIMOTO, Eisuke TATSUMI, Yoshiyuki TAENAKA

Key Words: Centrifugal Pump, Cardiopulmonary Support, Shear Stress, Pump Characteristics, Mechanical Trauma of Blood Cells

1　はじめに

膜型肺を用いた体外循環補助装置 (ECMO) 等の閉鎖型心肺補助装置は心肺停止状態患者の救急救命あるいは補助人工心臓等の高度治療へのつなぎとして非常に重要な装置である．この装置は主として遠心型血液ポンプ，膜型人工肺，静脈系に挿入され血液をポンプへ送る脱血カニューラ，ならびに動脈系に血液を還流させる送血カニューラから構成される．膜型人工肺の構造はガス交換に要する血液接触面積を最大にすべく直径数百 μm 程度の中空糸膜が 40% 以上の高密度で充填されており，その流路抵抗は無視できない．またカニューラについては挿入する血管のサイズに規定されるため，たとえば新生児 ECMO では脱血管先端が約 3mm といった例も存在し，大きな流路抵抗となる要素である．この場合には必然的にポンプに要求される発生圧力は高くなってしまい，使用する血液ポンプの設計次第では非常に高回転数下で運転されることによる血球の破壊が問題となりうる．本研究は，高圧力仕様のポンプとしてインペラを複数個直列に配した多段ポンプを新たに血液ポンプとして開発し，その基本的性能評価並びに問題点を明らかにすることを目的とする．

2　二段式遠心ポンプの設計

ポンプ設計にあたり，心肺補助装置の運転点をポンプ流量 3.0L/min, 500mmHg に設定した．また，市販されている心肺補助装置用のポンプ仕様を参考にし，市販製品より小型であるという条件に従いインペラの直径を 40mm，インペラ段数を 2 段として，一般の産業用遠心ポンプ設計法 [1] を参考にポンプ構成要素の設計を行った．Fig.1 に本ポンプの分解図を示す．血液はポンプ入口に設けたサクションボリュートを通過することにより第一段目のインペラに対し予旋回をもって流入する．このサクションボリュートは一段目羽根車の発生圧力を高める目的で設置されている．インペラは第一段と第二段で同一形状としており，それぞれ 4 枚の羽根を持ち，羽根出入口角はそれぞれ 4.7° と 80° である．また、戻り流路は 5 枚羽根によって形成され，羽根の入口角，出口角それぞれは 2° と 90° である．出口ケーシングとしてはインペラに作用する半径方向スラストを可能な限り低減するためにダブルボリュートとした．

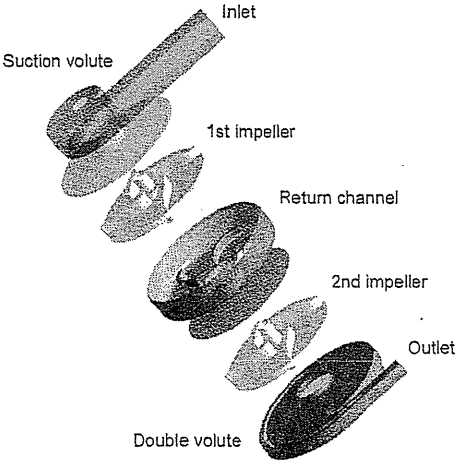

Fig. 1: Disassembled view of the blood pump

3　二段式遠心ポンプの性能試験

3.1　ポンプ特性　前述の設計に従って血液ポンプの試作を行った．血液ポンプは内部の圧力分布が計測できるよう圧力測定孔を多数有しており，回転軸以外の構成部品はすべてアクリル製とした．このポンプの水力学的特性を計測するために，ポンプを閉鎖回路に接続し，室温 (30°C) において生理食塩水を循環させ，抵抗の値を変化させながらポンプ流量とポンプ出入口部の各圧力値を計測した．また，駆動モータにはデジタルトルクメータを装着し，水力学的効率の算出に利用した．4200rpm において流量 5.0L/min で発生圧力 500mmHg を達成していることが示されている．また，最高効率は流量が約 5.0L/min のときに 29% を達成している．

3.2　圧力分布測定　本ポンプの特徴の一つは，第一段インペラにより圧力を得た流体を第二段に戻す役割を担う戻り流路の存在である．この戻り流路は第一段のインペラを出た流体の静圧を回復すると同時に第二段に入る流体の角速度をなくす役割を持つ．戻り流路の性能を含むポンプ内部の圧力変化を確認するために，ポンプの入口から出口までの圧力を測定した．

Fig.3 にポンプ内部の圧力測定位置を示す．ポンプの壁面近傍にセンサを配置することは困難であったため，圧力の時間変動は計測せず平均値のみで評価することとした．Fig.4 に圧力上昇の分布を示す．第一段，第二段の各インペラで同等の圧力上昇が実現できていることがわかる．また，戻り流路においては流量にほ

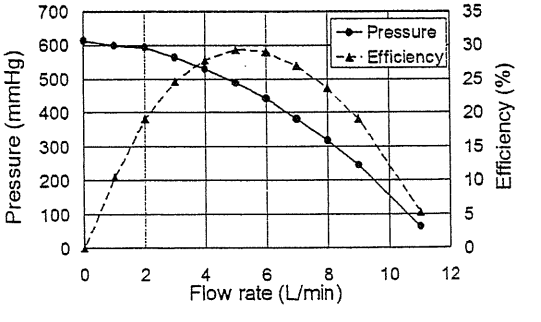

Fig. 2: Pump characteristics of the blood pump

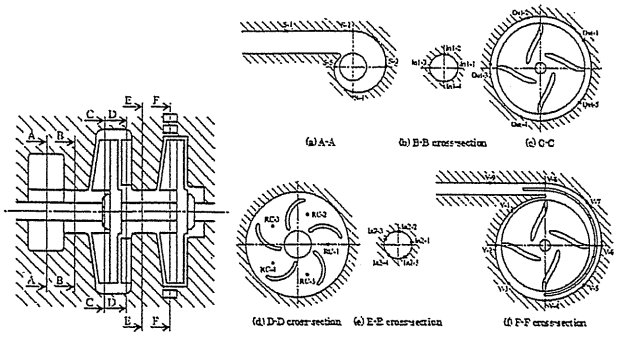

Fig. 3: The locations of the pressure measurement

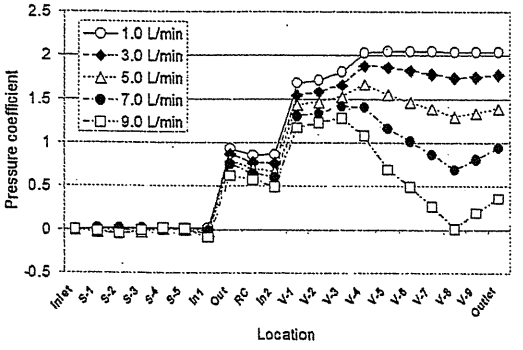

Fig. 4: The pressure distribution in the pump

とんど依存しない量の圧力損失が生じており，静圧への変換に伴う流体損失が発生していることが示されており，効率面からは戻り流路の改良が必要であることが示唆された．ポンプ出口に至るディフューザにおいては流量とともに増加する圧力損失が発生している．しかしながら設計流量である 3.0L/min では良好に圧力回復がなされており，設計が成功していることを示すものであると考えられる．

3.3 内部流れの数値シミュレーションに基づく改良　溶血や血栓形成が起こりうる場所を予想するため，汎用の熱流体解析ソフト ANSYS CFX-11.0 を用いて内部流れの非定常計算を行った．乱流モデルとして SST モデル，k-ω モデルを用いた．計算セルの形状は主に三角錐であり，壁面近傍では三角柱である．計算セル数は約 100 万である．この結果を利用してポンプ内部における流体力に起因する赤血球の破壊（溶血）を評価する血球破壊の発生については多くのモデルが提案されているがここでは血液に作用するせん断力が 200Pa を超えるかどうかで判断することとした [2]．血液を用いて運転する場合のレイノルズ数と水を用いた場合のレイノルズ数を一致させるため，動作流体を水として 1200rpm の条件で計算を行った．その場合にはせん断応力の閾値は約 16Pa となる．Fig.5 に一段目羽根車の翼端側ケーシング壁面におけるせん断応力分布を示す．本結果は乱流モデルとして $k-\omega$ モデルを用いたものであるが，ちょうど羽根翼端面が通過している部分にせん断応力が 16Pa を超える領域が発生していることが明らかとなった．これは翼の圧力面から負圧面に向かって羽根翼端面を乗り越える流れが発生していることによるものである．他にも，一段目羽根車バックシュラウド外縁，案内羽根外縁，二段目羽根車の翼端側ケーシング壁面，およびダブルボリュートの舌部において 16Pa 以上のせん断応力が発生していることが明らかとなった．また，流れが淀む領域では血液の凝固が発生し，血栓が形成されやすいと考えられるが，数値計算の結果，戻り流路の翼間において Fig6 に示す流れのベクトル図から明らかなように，流速の低い領域が形成されていることが判明した．

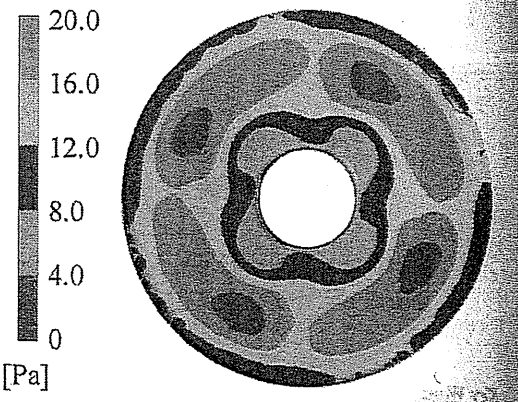

Fig. 5: The shear stress distribution on the casing wall near the 1st impeller of the pump

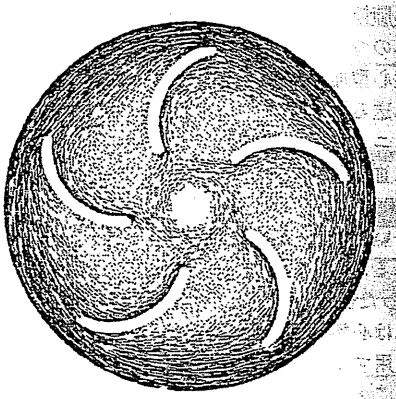

Fig. 6: The shear stress distribution on the casing wall near the 1st impeller of the pump

このように数値計算によって，血球の破壊ならびに血栓形成を防止する観点から，いくつかの設計変更を施す必要性が示唆された．今後主に数値計算によってポンプ各要素の形状改良の影響を明らかにし，本ポンプの改良モデルの製作，血液適合性に関する実験的検討へと開発を進めている予定である．

4 結　言

高い発生圧力を必要とする場合の心肺補助装置用の血液ポンプとして，従来応用例が見られなかった二段インペラを用いた多段遠心ポンプの開発を行った．産業ポンプの設計法を参考にして開発した第一次試作ポンプは，予定していた水力学的性能を実現することには成功したが，ポンプ内流れの数値流体解析を行った結果，血球の破壊あるいは血栓形成に関して改良すべき点が存在することが明らかとなった．

なお，本研究は平成 18，19 年度科学研究費補助金（基盤研究 (B)，課題番号：18360094）を利用して行われた．

参考文献

[1] 武田裕久，2005，「遠心ポンプの設計」，電業社機械，29(2) pp.7-14.

[2] Kameneva MV. et al., 2004, "Effects of Turbulent Stresses upon Mechanical Hemolysis: Experimental and Computational Analysis", ASAIO Journal, 50(5), pp.418-423.

141 空気駆動式補助人工心臓における機械式人工弁近傍での可視化研究

A Study on the Flow Visualization of a Mechanical Heart Valve in a Pneumatic Ventricular Assist Device

○非　李　桓成（国立循環器病センタ）、非　赤川英毅（国立循環器病センタ）、
正　簗谷朋典（国立循環器病センタ）、正　本間章彦（国立循環器病センタ）、
非　巽　英介（国立循環器病センタ）、非　妙中義之（国立循環器病センタ）

Hwansung Lee, National Cardiovascular Center, 5-7-1 Fujishiro-dai, Suita, Osaka
Eiki Akagawa, National Cardiovascular Center, 5-7-1 Fujishiro-dai, Suita, Osaka
Tomonori Tsukiya, National Cardiovascular Center, 5-7-1 Fujishiro-dai, Suita, Osaka
Akihiko Homma, National Cardiovascular Center, 5-7-1 Fujishiro-dai, Suita, Osaka
Eisuke Tatsumi, National Cardiovascular Center, 5-7-1 Fujishiro-dai, Suita, Osaka
Yoshiyuki Taenaka, National Cardiovascular Center, 5-7-1 Fujishiro-dai, Suita, Osaka

Our group is currently developing a pneumatic ventricular assist device (PVAD). In order to select the optimal bileaflet valve for our PVAD, in the current study we investigated the evolution of the flow field in a detailed time domain of three kinds of commercial bileaflet valves in our PVAD by means of the 2D particle image velocimetry method. To carry out flow visualization inside the blood pump and near the valve, we designed a model pump with the same configuration as our PVAD. Three kinds of bileaflet valves, the ATS valve, St. Jude valve and Sorin valve were mounted at the aortic position of the model pump and the flow was visualized by the PIV method. The maximum flow-velocity and Reynolds shear stress of the Sorin valve were less than those of the other two bileaflet valves. The Sorin valve has low Reynolds shear stress, and is considered the best valve for our PVAD among the three valves tested.

Key Words: < pneumatic ventricular assist device, bileaflet mechanical heart valve, flow visualization, particle image velocimetry >

背　景

心臓移植を要する心疾患数は、米国のみでも年間数万例に達すると推察されるが、実際の心臓移植症例数は年間 2,000 例にとどまっている(1)。その中、心臓移植へのブリッジとしては補助人工心臓（VAD）が広く使用されている。現在、拍動型補助人工心臓においては、補助人工心臓内部での血栓発生を防ぐために内部での洗い流し効果を得るため、一葉式機械弁が多く使用されている。しかし、現在に一葉式機械弁は臨床での使用は少なく、血流動力学的な特性に優れた二葉式機械弁が主に使用されている。我が国のみでも 2002 年の 1 年間で257 施設において臨床使用された人工弁の68%は機械弁であり、その中一葉式機械弁はわずか0.45%しか占めており(2)、将来には市販されない可能性が非常に高い。

本研究では、本施設で開発中の空気駆動式 VAD に最適な二葉式機械弁を調べるため、市販されている二葉式機械弁 3 種類を対象とし、弁周辺での流れの可視化より最大流速と最大レイノルズせん断応力を比較検討した。

実験方法

本施設では、空気駆動式 VAD を開発しており(3), 血液ポンプおよび弁周辺部での流れの可視化を行うため、実際の空気駆動式 VAD と同様な形状を持つモデルポンプをアクリルで製作した。モデルポンプはドノバン形模擬循環装置に接続し、補助循環装置（東洋坊、VCT-30）で駆動した。実験中、平均大動脈圧力は 100 mmHg にした。試験流体としては、アクリルと同一な屈折率を持つ 64%のヨウ化ナトリウム（粘度 3.3 cP、密度 1.9 g/cm^3 、20℃）を使用した。機械弁としては、直径 21 mm の ATS 弁、St. Jude 弁と Sorin 弁の 3 種類を対象とした(Fig. 1)。

流れの可視化は PIV システムを用いて行った。流れの解析には、可視化用解析ソフトを用い、トレーサには粒径 50 μm のポリスチレン粒子を用いた。

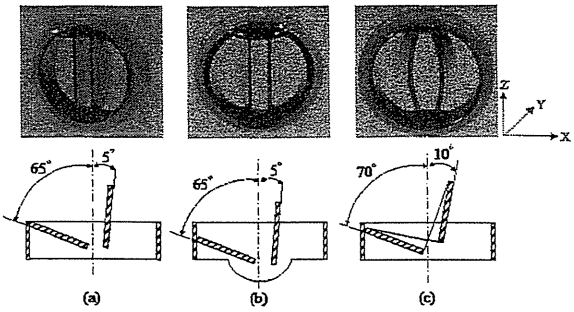

Fig.1 The bileaflet valves used in this study.

結果および考察

ATS 弁と St. Jude 弁においては、弁葉表面近くから速い流れが観察された。特に、ATS 弁では、壁付近で速い流速が観察された。一方、Sorin 弁では、弁葉表面および弁の下流から速い流れは観察されなかった(Fig. 2)。

ATS 弁では、X-Y 座標においては、ATS 弁で最大流速がもっとも速く最大 2.8 m/s であり、Sorin 弁でもっとも遅くなっていた。X-Z 座標においては、弁による最大速度の差は少なくなっていた(Fig.3)。

今研究の結果から弁周辺での流れは弁葉の形状によって異なっていた。特に、Sorin 弁においては、流速がもっとも遅くなっており、弁葉の形状が原因であると考えられる。また、最大レイノルズせん断応力はいずれの弁において弁葉付近で発生しており(Fig. 4)、Sorin 弁では ATS 弁と St. Jude 弁より小さくなっていた(Fig. 5)。ATS 弁と St. Jude 弁の弁葉の形状は平版形で

あり、血液ポンプの収縮期では弁周辺の流れは乱流になりやすく、最大レイノルズせん断応力が大きくなったと考えられる。一方、Sorin 弁の弁葉は曲面形であり、弁周辺の流れに対し抵抗が低くなり、最大流速と最大レイノルズせん断応力が少なくなったと思われる。

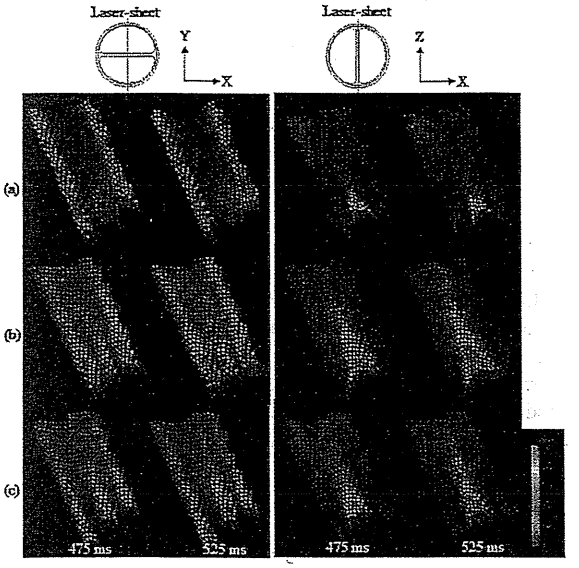

Fig. 2 Vector field of flow-velocity. (a) ATS valve, (b) St. Jude valve, (c) Sorin valve

結　論

本研究の結果より溶血の観点からでは Sorin 弁が当施設で開発した空気駆動式 VAD に最適であると考えられる。

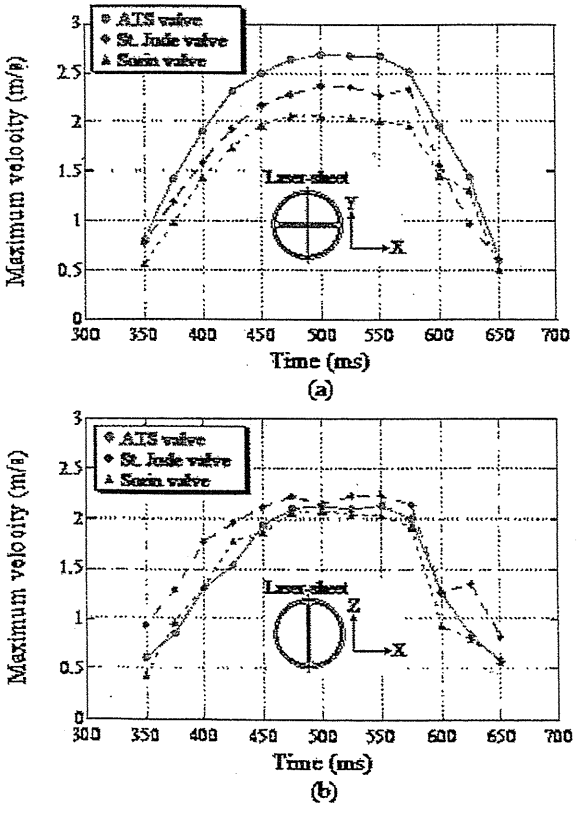

Fig.3 Maximum flow-velocity. (a) X-Y plane, (b) X-Z plane

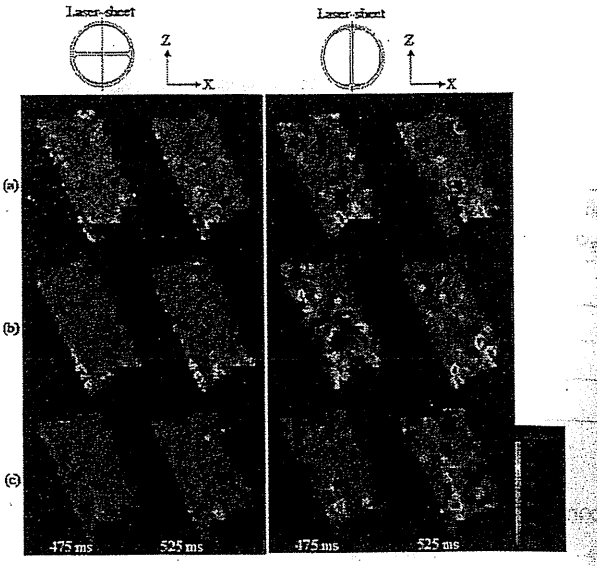

Fig.4 Reynolds shear stress field. (a) ATS valve, (b) St. Jude valve, (c) Sorin valve

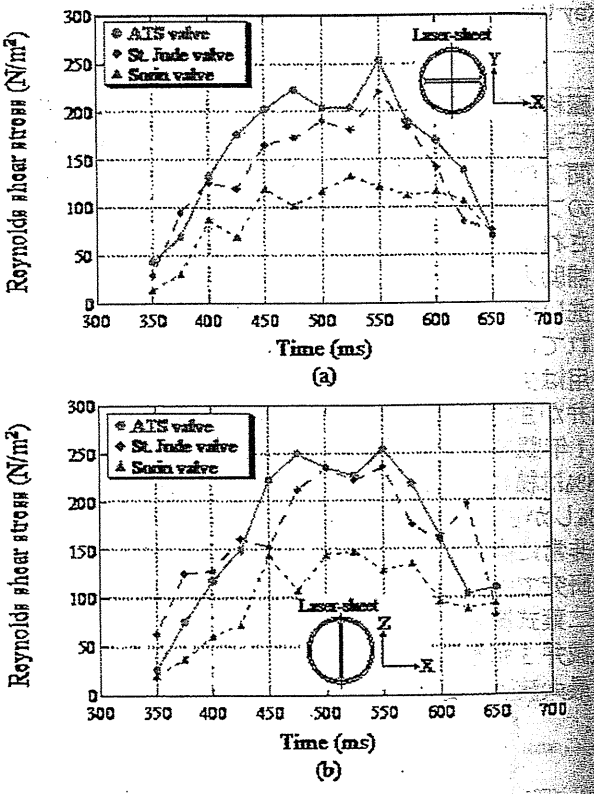

Fig.5 Mamimum Reynolds shear stress. (a) X-Y plane, (b) X-Z plane

参考文献

1. The United Network for Organs Sharing Web site. 2006.Available at www.unos.org Accessed February 22, 2006.
2. 人工臓器、Vol. 35別冊:5-11, 2006.
3. Akagawa E. et al. Effects of mechanical valve orifice direction on flow pattern in a ventricular assist device. J Artif Organs 10:85-91, 2007.

Am J Physiol Heart Circ Physiol 296: H1666–H1674, 2009.
First published February 27, 2009; doi:10.1152/ajpheart.01041.2008.

Angiotensin II disproportionally attenuates dynamic vagal and sympathetic heart rate controls

Toru Kawada,[1] Masaki Mizuno,[1] Shuji Shimizu,[2] Kazunori Uemura,[1] Atsunori Kamiya,[1] and Masaru Sugimachi[1]

[1]*Department of Cardiovascular Dynamics, Advanced Medical Engineering Center, National Cardiovascular Center Research Institute, Osaka and* [2]*Japan Association for the Advancement of Medical Equipment, Tokyo, Japan*

Submitted 29 September 2008; accepted in final form 25 February 2009

Kawada T, Mizuno M, Shimizu S, Uemura K, Kamiya A, Sugimachi M. Angiotensin II disproportionally attenuates dynamic vagal and sympathetic heart rate controls. *Am J Physiol Heart Circ Physiol* 296: H1666–H1674, 2009. First published February 27, 2009; doi:10.1152/ajpheart.01041.2008.—To better understand the pathophysiological role of angiotensin II (ANG II) in the dynamic autonomic regulation of heart rate (HR), we examined the effects of intravenous administration of ANG II (10 $\mu g \cdot kg^{-1} \cdot h^{-1}$) on the transfer function from vagal or sympathetic nerve stimulation to HR in anesthetized rabbits with sinoaortic denervation and vagotomy. In the vagal stimulation group ($n = 7$), we stimulated the right vagal nerve for 10 min using binary white noise (0–10 Hz). The transfer function from vagal stimulation to HR approximated a first-order low-pass filter with pure delay. ANG II attenuated the dynamic gain from 7.6 ± 0.9 to 5.8 ± 0.9 beats$\cdot min^{-1} \cdot Hz^{-1}$ (means ± SD; $P < 0.01$) without affecting the corner frequency or pure delay. In the sympathetic stimulation group ($n = 7$), we stimulated the right postganglionic cardiac sympathetic nerve for 20 min using binary white noise (0–5 Hz). The transfer function from sympathetic stimulation to HR approximated a second-order low-pass filter with pure delay. ANG II slightly attenuated the dynamic gain from 10.8 ± 2.6 to 10.2 ± 3.1 beats$\cdot min^{-1} \cdot Hz^{-1}$ ($P = 0.049$) without affecting the natural frequency, damping ratio, or pure delay. The disproportional suppression of the dynamic vagal and sympathetic regulation of HR would result in a relative sympathetic predominance in the presence of ANG II. The reduced high-frequency component of HR variability in patients with cardiovascular diseases, such as myocardial infarction and heart failure, may be explained in part by the peripheral effects of ANG II on the dynamic autonomic regulation of HR.

systems analysis; transfer function; heart rate variability; cardiac sympathetic nerve activity; rabbit

AUTONOMIC NERVOUS ACTIVITY changes dynamically during daily activity, and thus the dynamic heart rate (HR) regulation by the autonomic nervous system is physiologically important. The high-frequency (HF) component of HR variability (HRV) is thought to reflect primarily vagal nerve activity, because the vagal nerve can change the HR more quickly than the sympathetic nerve (1, 3, 14, 34). This does not mean, however, that the sympathetic system cannot affect the HF component. For example, an increase in background sympathetic tone augments the HR response to vagal stimulation, an effect that has been referred to as accentuated antagonism (20). In accordance with accentuated antagonism, selective cardiac sympathetic nerve stimulation augments the dynamic HR response to vagal stimulation (14). On the other hand, high plasma concentration of norepinephrine (NE) with no direct activation of the cardiac sympathetic nerve attenuates the dynamic HR response to vagal stimulation via an α-adrenergic mechanism (24). These results suggest that the sympathetic system can influence the HF component via complex interactions with the vagal system.

During systemic sympathetic activation, the renin-angiotensin system is activated through stimulation of β_1-adrenergic receptors on juxtaglomerular granular cells (8, 12). In such conditions as hypertension, myocardial ischemia, and heart failure, the renin-angiotensin system and the sympathetic nervous system are both activated (9, 35). Previous studies demonstrated that acute intravenous or intracerebroventricular administration (32) or chronic intravenous administration of angiotensin II (ANG II) modified the baroreflex control of HR in rabbits (5), possibly via a decrease in vagal tone and an increase in sympathetic tone to the heart. In the present study, we focused on the peripheral effects of ANG II and examined the effects of intravenous ANG II on the dynamic HR response to vagal or postganglionic cardiac sympathetic nerve stimulation. In a previous study from our laboratory where anesthetized cats were used, intravenous ANG II (10 $\mu g \cdot kg^{-1} \cdot h^{-1}$) attenuated myocardial interstitial acetylcholine (ACh) release in response to vagal nerve stimulation (17); therefore, we hypothesized that intravenous ANG II at this dose would attenuate the dynamic HR response to vagal nerve stimulation. On the other hand, a previous study from our laboratory where anesthetized rabbits were used demonstrated that intravenous ANG II at a similar dose of 6 $\mu g \cdot kg^{-1} \cdot h^{-1}$ did not affect the peripheral arc transfer function estimated between renal sympathetic nerve activity and arterial pressure (AP) (13). Accordingly, we hypothesized that intravenous administration of ANG II would not modulate the dynamic sympathetic control of HR significantly. We focused on the relative effects of ANG II on the vagal and sympathetic HR regulations because the balance between vagal and sympathetic nerve activities would be a key to understanding the pathophysiology of several cardiovascular diseases.

MATERIALS AND METHODS

Surgical preparations. Animal care was performed in accordance with *Guideline Principles for the Care and Use of Animals in the Field of Physiological Sciences*, which has been approved by the Physiological Society of Japan. All experimental protocols were reviewed and approved by the Animal Subjects Committee at the National Cardiovascular Center. Twenty-one Japanese white rabbits weighing 2.4–3.4 kg were anesthetized with intravenous injections (2 ml/kg) of a mixture of urethane (250 mg/ml) and α-chloralose (40 mg/ml) and mechanically ventilated with oxygen-enriched room air. A double-lumen catheter was inserted into the right femoral vein, and a supplemental dose of the anesthetics was given continuously (0.5–1.0

Address for reprint requests and other correspondence: T. Kawada, Dept. of Cardiovascular Dynamics, Advanced Medical Engineering Center, National Cardiovascular Center Research Institute, 5-7-1 Fujishirodai, Suita, Osaka 565-8565, Japan (e-mail: torukawa@res.ncvc.go.jp).

$ml \cdot kg^{-1} \cdot h^{-1}$). AP was monitored using a micromanometer catheter (Millar Instruments, Houston, TX) inserted into the right femoral artery. HR was determined from the electrocardiogram using a cardiotachometer. Sinoaortic denervation and vagotomy were performed bilaterally to minimize reflex changes in efferent sympathetic nerve activity. The left and right cardiac sympathetic nerves were exposed using a midline thoracotomy and sectioned (16). In the vagal stimulation group, a pair of bipolar stainless steel wire electrodes was attached to the cardiac end of the sectioned right vagal nerve for stimulation. A pair of stainless steel wire electrodes was attached to the proximal end of the sectioned right cardiac sympathetic nerve for recording efferent cardiac sympathetic nerve activity (CSNA). In the sympathetic stimulation group, a pair of bipolar stainless steel wire electrodes was attached to the cardiac end of the sectioned right sympathetic nerve for stimulation. Efferent CSNA was recorded from the proximal end of the sectioned left cardiac sympathetic nerve. The preamplified nerve signal was band-pass filtered between 150 and 1,000 Hz. The signal was then full-wave rectified and low-pass filtered with a cut-off frequency of 30 Hz to quantify the nerve activity. Both the stimulation and recording electrodes were fixed to the nerve by addition-curing silicone glue (Kwik-Sil; World Precision Instruments, Sarasota, FL). We confirmed that the recorded CSNA was mainly postganglionic by observing the disappearance of CSNA following intravenous administration of hexamethonium bromide (50 mg/kg) at the end of each experiment. The body temperature of the animal was maintained at 38°C with a heating pad throughout the experiment.

Protocols. In the vagal stimulation group (n = 7), the stimulation amplitude was adjusted (3–6 V) in each animal to yield a HR decrease of ~50 beats/min at 5-Hz tonic stimulation with a pulse duration of 2 ms. To estimate the transfer function from vagal stimulation to HR, a random vagal stimulus was applied for 10 min by altering the stimulus command every 500 ms at either 0 or 10 Hz according to a binary white noise signal. The input power spectral density was relatively constant up to 1 Hz, which covered the upper frequency range of interest with respect to the vagal transfer function in rabbits (26).

In the sympathetic stimulation group (n = 7), the stimulation amplitude was adjusted (1–3 V) in each animal to yield a HR increase of ~50 beats/min at 5-Hz tonic stimulation with a pulse duration of 2 ms. To estimate the transfer function from sympathetic stimulation to HR, a random sympathetic stimulus was applied for 20 min by altering the stimulus command every 2 s at either 0 or 5 Hz according to a binary white noise signal. The input power spectral density was relatively constant up to 0.25 Hz, which covered the upper frequency range of interest with respect to the sympathetic transfer function in rabbits (15).

In both the vagal stimulation and sympathetic stimulation groups, the dynamic HR response to nerve stimulation was first recorded under conditions of continuous intravenous infusion of physiological saline solution ($1\ ml \cdot kg^{-1} \cdot h^{-1}$). After the control data were recorded, nerve stimulation was stopped and ANG II was intravenously administered at $10\ \mu g \cdot kg^{-1} \cdot h^{-1}$ ($1\ ml \cdot kg^{-1} \cdot h^{-1}$ of 10 μg/ml solution) instead of the physiological saline solution. After 15 min, we repeated the random stimulation of the vagal or sympathetic nerve while continuing the intravenous injection of ANG II. We used the same binary white noise sequence for the control and ANG II conditions in each animal and changed the sequence for different animals.

In a supplemental protocol (n = 7), we examined the time effect on the estimation of the sympathetic transfer function. The 20-min random sympathetic stimulation was repeated twice with an intervening interval of more than 20 min.

Data analysis. Data were digitized at 200 Hz using a 16-bit analog-to-digital converter and stored on the hard disk of a dedicated laboratory computer system. Prestimulation values of HR, AP, and CSNA were calculated by averaging data obtained during the 10 s immediately before nerve stimulation. The mean HR and AP values in response to nerve stimulation were calculated by averaging data obtained during the nerve stimulation period. The mean level of CSNA during the nerve stimulation period was not evaluated because contamination from stimulation artifacts could not be completely eliminated.

The transfer function from nerve stimulation to the HR response was estimated as follows. The input-output data pairs of nerve stimulation and HR were resampled at 10 Hz. To avoid the initial transition from no stimulation to random stimulation biased the transfer function estimation, data were processed only from 2 min after the initiation of random stimulation. In the vagal stimulation group, the data were divided into eight segments of 1,024 data points that half-overlapped with neighboring segments. In the sympathetic stimulation group, the data were divided into eight segments of 2,048 data points that half-overlapped with neighboring segments. For each segment, a linear trend was subtracted and a Hanning window was applied. We then performed a fast Fourier transformation to obtain the frequency spectra of the stimulation command [$X(f)$] and HR [$HR(f)$] (4). We calculated ensemble averages of the power spectral densities of the stimulation command [$S_{X \cdot X}(f)$] and HR [$S_{HR \cdot HR}(f)$] and the cross spectral density between the two signals [$S_{HR \cdot X}(f)$]. Finally, we obtained the transfer function [$H(f)$] from the nerve stimulation to HR response using the following equation (23):

$$H(f) = \frac{S_{HR \cdot X}(f)}{S_{X \cdot X}(f)}$$

To quantify the linear dependence of the HR response to vagal or sympathetic nerve stimulation, we estimated the magnitude-squared coherence function [$Coh(f)$] using the following equation (23):

$$Coh(f) = \frac{|S_{HR \cdot X}(f)|^2}{S_{X \cdot X}(f) \cdot S_{HR \cdot HR}(f)}$$

The coherence function ranges zero and unity and indicates a frequency-domain measure of linear dependence between input and output variables.

Because previous studies found that the transfer function from vagal stimulation to HR approximated a first-order low-pass filter with pure delay (14, 24), we determined the parameters of the vagal transfer function using the following model:

$$H_{vagus}(f) = -\frac{K}{1 + \frac{f}{f_C} j} e^{-2\pi f j L}$$

where K is dynamic gain (in $beats \cdot min^{-1} \cdot Hz^{-1}$), f_C is the corner frequency (in Hz), and L is pure delay (in s). Variables f and j represent frequency and an imaginary unit, respectively. The minus sign in the right side of the equation corresponds to the negative HR response to vagal stimulation.

Because previous studies suggested that the transfer function from sympathetic stimulation to HR approximated a second-order low-pass filter with pure delay (14, 28), we determined the parameters of the sympathetic transfer function using the following model:

$$H_{symp}(f) = \frac{K}{1 + 2\zeta \frac{f}{f_N} j + \left(\frac{f}{f_N} j\right)^2} e^{-2\pi f j L}$$

where K is dynamic gain (in $beats \cdot min^{-1} \cdot Hz^{-1}$), f_N is the natural frequency (in Hz), ζ is the damping ratio, and L is pure delay (in s).

Because deviation of the model transfer function [$H_{model}(f)$] from the estimated transfer function [$H_{est}(f)$] would affect the transfer function parameters, we assessed the goodness of fit using the following equation: